



Immobilizing c(RGDfc) on the surface of metal-phenolic networks by thiol-click reaction for accelerating osteointegration of implant

Zeyu Shou^{a,d}, Zhibiao Bai^a, Kaiyuan Huo^e, Shengwu Zheng^f, Yizhe Shen^a, Han Zhou^a, Xiaojing Huang^a, Hongming Meng^a, Chenwei Xu^a, Shaohao Wu^a, Na Li^{d,**}, Chun Chen^{a,b,c,*}

^a Department of Orthopedics, The First Affiliated Hospital of Wenzhou Medical University, Wenzhou, 325000, People's Republic of China

^b Key Laboratory of Intelligent Treatment and Life Support for Critical Diseases of Zhejiang Province, Wenzhou, 325000, Zhejiang, People's Republic of China

^c Zhejiang Engineering Research Center for Hospital Emergency and Process Digitization, Wenzhou, Zhejiang, 325000, People's Republic of China

^d Wenzhou Institute, University of Chinese Academy of Sciences, Wenzhou, 325001, People's Republic of China

^e School of Pharmaceutical Sciences, Wenzhou Medical University, Wenzhou, 325000, People's Republic of China

^f Wenzhou Celecare Medical Instruments Co., Ltd, Wenzhou, 325000, People's Republic of China

ARTICLE INFO

Keywords:

Implant surface
Peptide immobilization
Arginyl-glycyl-aspartic (RGD)
Metal-phenolic networks (MPNs)
Osteointegration

ABSTRACT

The limited osteointegration often leads to the failure of implant, which can be improved by fixing bioactive molecules onto the surface, such as arginyl-glycyl-aspartic acid (RGD): a cell adhesion motif. Metal-Phenolic Networks (MPNs) have garnered increasing attention from different disciplines in recent years due to their simple and rapid process for depositing on various substrates or particles with different shapes. However, the lack of cellular binding sites on MPNs greatly blocks its application in tissue engineering. In this study, we present a facile and efficient approach for producing PC/Fe@c(RGDfc) composite coatings through the conjugation of c(RGDfc) peptides onto the surface of PC/Fe-MPNs utilizing thiol-click reaction. By combined various techniques (ellipsometry, X-ray photoelectron spectroscopy, Liquid Chromatography-Mass Spectrometry, water contact angle, scanning electronic microscopy, atomic force microscopy) the physicochemical properties (composition, coating mechanism and process, modulus and hydrophilicity) of PC/Fe@c(RGDfc) surface were characterized in detail. In addition, the PC/Fe@c(RGDfc) coating exhibits the remarkable ability to positively modulate cellular attachment, proliferation, migration and promoted bone-implant integration in vivo, maintaining the inherent features of MPNs: anti-inflammatory, anti-oxidative properties, as well as multiple substrate deposition. This work contributes to engineering MPNs-based coatings with bioactive molecules by a facile and efficient thiol-click reaction, as an innovative perspective for future development of surface modification of implant materials.

1. Introduction

The limited tissue-binding and regenerative potential on the surface often lead to poor osteointegration and the failure of orthopedic implants [1]. The interfacial interaction between an implant and its surrounding biological environment plays a critical role on the outcomes of the implant [2]. Grafting bioactive molecules, such as growth factors [3], and extracellular matrix-like protein [4,5], etc., onto implant surfaces to provide necessary bio-signals for osteointegration was demonstrated as one of the potent strategies for improving implant osteointegration. However, due to the fragility of bioactive molecules,

an environmentally friendly, efficient, and simple yet versatile strategies for immobilizing is still highly pursuit.

Metal-polyphenol networks (MPNs) formed by metal ions and phenolic ligands [6,7] have garnered increasing attention from different disciplines in recent years due to their simple and rapid process to deposit on various substrates or particles with different shapes [8,9], since reported by Caruso et al. The wide range of applicable metal ions [10] (Fe^{3+} , Cu^{2+} , Mg^{2+} , etc.), the large family of polyphenols [11] (more than 8000 species of polyphenols have been identified), selective permeability, stimuli responsiveness and good thermal stability, make MPNs very promising in drug delivery [12], bioactive coating [13],

* Corresponding author. Department of Orthopedics, The First Affiliated Hospital of Wenzhou Medical University, Wenzhou, 325000, People's Republic of China.

** Corresponding author.

E-mail addresses: lina0701@ucas.ac.cn (N. Li), chenchunkk@163.com (C. Chen).

<https://doi.org/10.1016/j.mtbio.2024.101017>

Received 5 December 2023; Received in revised form 14 February 2024; Accepted 2 March 2024

Available online 3 March 2024

2590-0064/© 2024 The Authors. Published by Elsevier Ltd. This is an open access article under the CC BY-NC license (<http://creativecommons.org/licenses/by-nc/4.0/>).

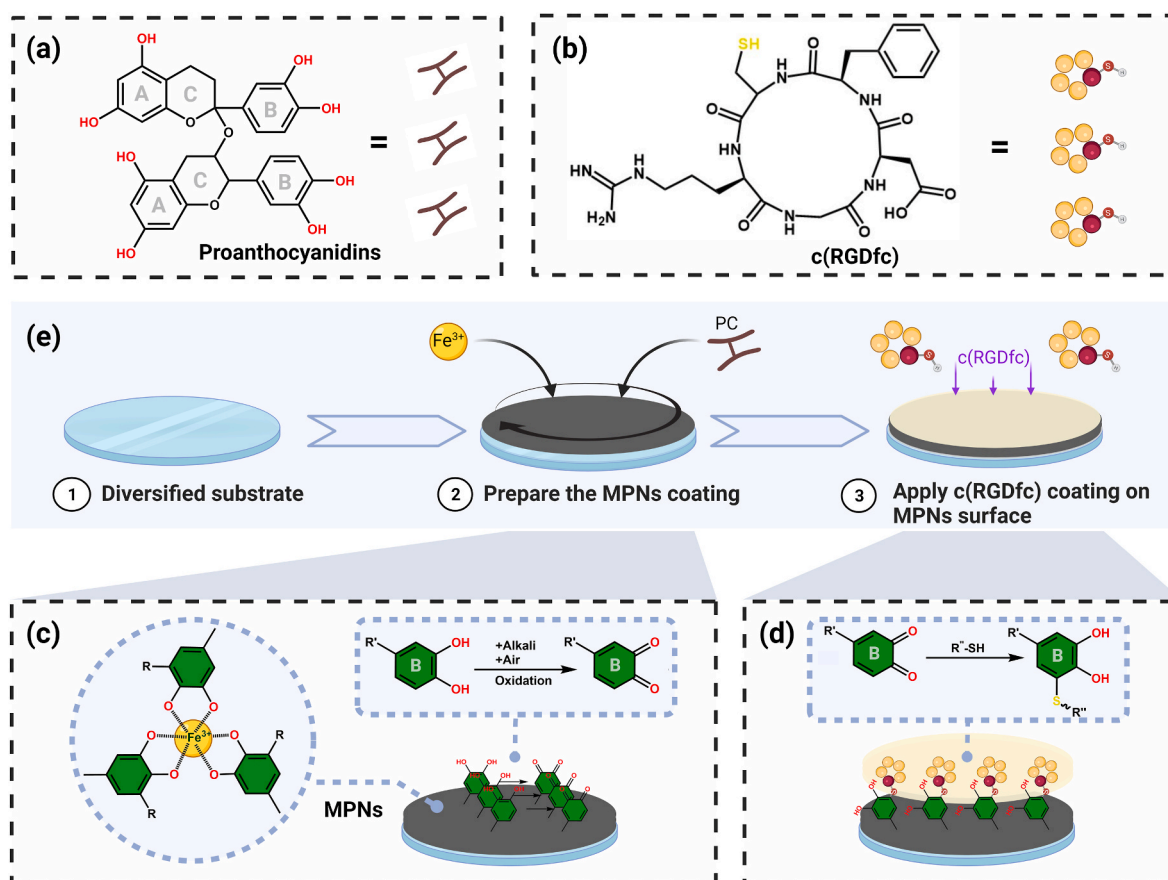
environmental engineering [14] and daily life [15], etc. Recently, MPNs have been designed as multifunctional implant coatings because they retain the inherent functions of polyphenols and metal ions. For example, Huang et al. explored the MPNs formed by tannic acid (TA)/catecholamine and Cu (II) for potential cardiovascular applications because of their synergistic anti-inflammatory, antibacterial, and anticoagulant properties [16]. Asgari et al. put forward a Mg-phenolic network strategy aimed at bolstering the corrosion resistance and osteo-compatibility of degradable Mg alloys through adjustment of the Mg concentration in the coating [17].

It is noteworthy that Ding et al., after a careful discussion, proposed that the polydopamine (PDA) coating caused a decrease in cell viability in standard tests, which was caused by the energy consumption caused by the intensified local motility of cells [18]. Similar to the PDA coating, our experiments and the results of some published papers show that MPNs-coated surface is not a very effective surface. During the culture process of cells on MPNs-coated surfaces, there is no significantly enhanced cell viability [17], migration [19], and adhesion capacity [20]. This may be caused by the lack of cell recognition and binding sites [21]. Therefore, how to graft bioactive molecules on the surface of MPNs to improve their biocompatibility is a question worth exploring. In the past decade, biomaterials designed based on DOPA or MPNs have been extensively explored. Among them, Li et al. used physical adsorption to link growth factors on the TA/Fe-MPNs surface to enhance the cell interaction at the implant interface. However, physical adsorption often leads to drug exfoliation due to weak non-covalent bonds and is unable to play long-term bioactivity [22]. Chemical grafting on the coating surface is a feasible method [23], but Chemical grafts often rely on the molecular design and harsh conditions. Still need to create a simple,

mild, universal, and cost-effective approach to construct bioactive interfaces. Among which the click reaction provides a new idea for the immobilization of bioactive molecules due to its mild and direct reaction conditions, fast reaction rate, and strong specificity [24]. Some researchers have achieved efficient grafting of multiple types of peptides by clicking dibenzylcyclooctyne (DBCO)-capped peptides onto the surface of DOPA-N3-coated materials [25,26]. However, click reactions have not been reported on the surface of more functional MPNs.

Peptide sequences with minimal structural domains are a hot research topic in the biomedical materials field as they exhibit excellent biocompatibility and biodegradability [27]. The glycine-arginine-aspartic acid (RGD) peptides, which are specific amino acid sequences found in extracellular matrices (ECMs), are the most commonly used and effective pro-adhesion peptides [28]. Among them, cyclo-(Arg-Gly-Asp-D-Phe-Cys) (c(RGDfc)) is an affordable and widely available modified variant of the RGD sequence, with a D-Phe and Cys residues added to its C-terminus to form a ring structure, which also introduces a thiol group on the molecule [29,30]. Some studies have shown that, due to this loop structure, compound c(RGDfc) peptide on the surface of materials can more effectively and non-specifically bind to various integrin receptors on cell membranes and induce cellular integrin gene expression, promote cell adhesion, and differentiate and mature [31,32]. Meanwhile, the c(RGDfc) ring structure increases its stability and biocompatibility in biological materials [33].

In this study, PC/Fe@c(RGDfc) composite coatings were innovatively constructed by grafting c(RGDfc) on the surface PC/Fe-MPNs using click reaction (Scheme 1). Among them, proanthocyanidins (PC) as a mature coating construction strategy has been extensively studied by our research group [34–36]. Here PC/Fe-MPNs as a multifunctional



Scheme 1. (a) The structure of PC and its schematic diagram, (b) the structure of c(RGDfc) and its schematic diagram, (c) the construction of MPN and its oxidation in alkaline environment, (d) the reaction of the sulfhydryl group of cysteine on c(RGDfc) with MPN under alkaline conditions, (e) the schematic diagram of the construction of PC/Fe@c(RGDfc) composite coating on various substrates. Created with [BioRender.com](https://www.biorender.com).

building block, serving three distinct roles: (i) providing versatile substrate modification through its adhesive properties, (ii) acting as a platform for immobilizing c(RGDfc), and (iii) functioning as an intermediate layer with notable antioxidant activity [37]. While c(RGDfc) provides cell-recognizable sites for PC/Fe@c(RGDfc) composite coating, modified PC/Fe-MPNs serve as an efficient tissue-integrated interface. Our research demonstrates that the PC/Fe@c(RGDfc) composite coating not only enhanced the biomedical properties of MPNs such as cell adhesion, proliferation, migration, and anti-oxidation in vitro, but also improved host tissue integration and mechanical fixation.

2. Materials and methods

2.1. Main materials

Proanthocyanidins (PC, Cas: 4852-22-6), iron(III) nitrate nonahydrate ($\text{Fe}(\text{NO}_3)_3 \cdot 9\text{H}_2\text{O}$, Cas: 7782-61-8) were obtained from Macklin, anhydrous sodium acetate (Cas: 127-09-3) and tris(hydroxymethyl)aminomethane (Tris, Cas: 1185-53-1) were obtained from aladdin. The c(RGDfc) peptide was purchased from Hangzhou All Peptide Biotechnology Co., Ltd. Fetal bovine serum (FBS), Dulbecco's modified Eagle's medium (DMEM) and Minimum Essential Medium Eagle (MEM) were purchased from Gibco. 4% paraformaldehyde, Triton X-100, rhodamine phalloidin (phalloidin-TRITC), and polypropylene (PP) sheets were purchased from Sigma. 6-diamidino-2-phenylindole (DAPI), Cell Counting Kit-8 (CCK-8), and the ROS assay kit and ferric reducing antioxidant capacity (FRAP) assay kit were purchased from Dojindo Laboratories and Beyotime Institute of Biotechnology. Vitreous cell culture plates (Cas: 801004) were purchased from NEST Biotechnology. Other cell culture consumables, such as cell culture dishes (Cas: TCD000035) and centrifuge tubes (Cas: CFT312150), were purchased from Guangzhou Jet Bio-Filtration Co., Ltd. All chemicals were used without further purification. Silicon wafers (SSPs), quartz plates (Alfa Aesar), and round glass coverslips (14 mm diameter, NEST) were washed with piranha solution (70% H_2SO_4 and 30% H_2O_2 , V/V) at 98 °C for 2 h, followed by rinsing with Milli-Q water, and drying in a mild air stream before use (Caution: Piranha solution is highly oxidizing and corrosive and should be prepared and used with extreme caution). The deionized (DI) water used in the experiments was purified using the Milli-Q system, providing a resistivity greater than 18.25 M Ω cm.

2.2. Preparation of PC/Fe-MPNs and PC/Fe@c(RGDfc)

PC/Fe@c(RGDfc) hybrid coating comprising of PC/Fe-MPNs coating and c(RGDfc) peptide was synthesized using a two-step method in aqueous media at room temperature (Scheme 1): fabricating PC/Fe-MPNs coating and following conjugation of c(RGDfc) onto PC/Fe-MPNs coating.

2.2.1. Preparation of the PC/Fe-MPNs coating

The PC/Fe-MPNs coating was prepared according to the procedure already reported [34,35]. In detail, PC was dissolved in acetic acid sodium acetate buffer solution (10 mM, pH 4.5) to obtain a solution with a concentration of 0.5 mM. $\text{Fe}(\text{NO}_3)_3$ was dissolved in DI water to obtain a solution of 1.5 mM. As shown in Scheme 1c, the MPN coating preparation occurred within a 5 mL tube housing a clean silicon wafer substrate measuring 1 cm \times 1 cm. Initially, 1 mL of the PC solution was added swiftly by 1 mL of the $\text{Fe}(\text{NO}_3)_3$ solution (in less than 10 s). The mixture was vigorously vortexed for 30 s and left undisturbed for 10 min. Subsequently, 1 mL Tris-HCl buffer solution (0.3 M, pH 8) was added and mixed for 30 s to stabilize the membrane structure. Finally, the PC/Fe-MPNs coated substrate was carefully rinsed with DI water and mildly dried with an air stream. This deposition process was repeated until the desired thickness of the MPN coating was achieved, denoted as (PC/Fe)_x-MPNs, where x was the number of cycles.

2.2.2. Preparation of the PC/Fe@c(RGDfc) coating

The c(RGDfc) peptide was dissolved in Tris-HCl buffer solution (10 mM, pH = 8.5) to obtain a solution with a concentration of 1 mg/mL. As shown in Scheme 1d, the preparation process of the PC/Fe@c(RGDfc) coating was carried out in a 5 mL tube that contained a substrate coated with PC/Fe-MPNs (1 cm², 5 or 10 layers), to which the c(RGDfc) solution was added and left for 24 h. The PC/Fe@c(RGDfc) coated substrate was then rinsed with DI water and dried gently with an air stream, resulting in stable PC/Fe@c(RGDfc) coatings. In the subsequent experiments, based on the previous work [35,38], we selected PC/Fe@c(RGDfc) coatings based on 5 layers MPN for in vivo and in vitro experiments.

2.3. Characterization

The as-prepared MPN coatings were stored at 4 °C and thoroughly dried before undergoing any characterization. The thickness of the coatings was determined using optical ellipsometry (M-2000UI, J.A. Woollam). Surface morphologies were examined using a scanning electron microscope (SEM) (SU8010, Hitachi). X-ray photoelectron spectroscopy (XPS) spectra of silicon wafer-coated MPN samples were obtained using a Thermo-Electron ESCALAB 250 spectrometer equipped with a monochromatic Al X-ray source (1486.6 eV). Liquid Chromatography-Mass Spectrometry (1290 Infinity II+ 6135MS, Agilent, USA) obtained MS mass spectra of c(RGDfc), c(RGDfc) + PC, and +PC after alkylation of c(RGDfc) with 1 mM iodoacetamide (Cas: 144-48-9, Macklin). Water contact angle (WCA) analyses were performed using the static sessile drop method on a KRUSS DSA1 version 1.80 drop shape analyzer with water as the probe liquid. The zeta potentials of PC/Fe-MPNs and PC/Fe@c(RGDfc) coatings on the surface of PS beads ($\varphi = 3\mu\text{m}$) were measured using a Zetasizer Nano ZS ZEN3600 (WM2016002, Malvern).

2.3.1. Factors of PC/Fe@c(RGDfc) fabrication

The fabrication of PC/Fe@c(RGDfc) coatings was investigated with regard to pH, c(RGDfc) concentration, deposition time, and thickness of PC/Fe-MPNs. Tris (10 mM) was utilized to adjust the pH values of the c(RGDfc) solution to 7, 7.5, 8, 8.5 and 9. The concentration of the c(RGDfc) solution was adjusted to 0.01, 0.1, and 1 mg/mL using Tris-HCl buffer with a fixed pH. By extending the introduction time of the c(RGDfc) solution onto the PC/Fe-MPNs coating, PC/Fe@c(RGDfc) coatings with varying deposition times were obtained. Additionally, by increasing the cycle number of the PC/Fe-MPNs coating, surfaces grafted with c(RGDfc) peptide with different thicknesses were achieved.

2.3.2. Decomposition process of PC/Fe@c(RGDfc)

The decomposition process of PC/Fe@c(RGDfc) was conducted by immersing a substrate coated with PC/Fe@c(RGDfc) into PBS solution (pH 7.3), 0.9% NaCl solution, DMEM medium and DMEM containing trypsin (0.5 mg/mL) for the desired duration (0–14 days). Subsequently, the sample was washed with DI water and dried under vacuum. The thickness of the coating was measured using optical ellipsometry.

2.3.3. Free radical scavenging assays

The total antioxidant capacity of the coatings was assessed using the Total Antioxidant Capacity Assay Kit with the FRAP method. Firstly, a working curve was established according to the protocol provided by the FRAP assay kit. FeSO_4 solutions with specific concentrations (0, 0.15, 0.3, 0.6, 0.9, 1.2, and 1.5 mM) were prepared and added to a 96-well plate, followed by the addition of the working solution (180 μL). After incubating for 5 min at 37 °C, the absorbance of the 96-well plate was measured at 593 nm using a spectrophotometer. The total antioxidant activities of the coatings, glass, and Trolox solution (1 mM) were determined immediately after preparation and after two months of storage, following the same procedure. Glass and Trolox served as the negative and positive control, respectively. Based on the measured intensities, the antioxidant activity of each sample was calibrated using

the standard curve.

The DPPH radical scavenging activity of the coatings was determined using the DPPH radical scavenging Capacity Assay Kit (Cas: BC4750, Solarbio). Briefly, glass, VC (0.3 mg/mL), PC/Fe-MPNs, and PC/Fe@c(RGDfc) coatings (50 nm, 2 cm²) were mixed with the working solution. The absorbance at 515 nm was obtained using a Lambda 25 spectrophotometer from PerkinElmer. The calculation formula for the DPPH radical scavenging rate of the samples is as follows

$$\text{DPPH inhibition rate (\%)} = \left[\text{Abs blank} - \frac{\text{Abs control} - \text{Abs sample}}{\text{Abs blank}} \right] \times 100\%$$

The ABTS radical scavenging activity of the PC coatings was determined using the ABTS radical scavenging Capacity Assay Kit (Cas: BC4770, Solarbio). Briefly, glass, VC (1.5 mM), PC/Fe-MPNs, and PC/Fe@c(RGDfc) coatings (50 nm, 2 cm²) were mixed with the assay kit's working solution. The absorbance at 405 nm was obtained using a Lambda 25 spectrophotometer from PerkinElmer. The calculation formula for the ABTS radical scavenging rate of the samples is as follows

$$\text{ABTS inhibition rate (\%)} = \left[\text{Abs blank} - \frac{\text{Abs control} - \text{Abs sample}}{\text{Abs blank}} \right] \times 100\%$$

2.4. Cell culture

The NIH3T3 (Cas: CL-0171) and the Human umbilical vein endothelial cells (HUVECs, Cas: CP-H082) were purchased from Pricella Life Science&Technology Co.,Ltd and cultured in Cell Culture Bottle (75 mL volume) in DMEM medium (Gibco, 8123125, Waltham, USA) with 10% FBS (Gibco, 16000044, Waltham, USA). Bone-marrow mesenchymal stem cells (BMSCs) were isolated from the bone marrow of SPF C57BL/6 mice aged 3 weeks as the previous study described [39]. The BMSCs were planted on Cell Culture Bottle (75 mL volume) in MEM medium (Gibco, 2276722, Waltham, USA) with 10% FBS. All the cells were maintained in a humidified incubator with an atmosphere of 37 °C and 5% CO₂. The medium was replaced every 2–3 days. The cells were passaged with 0.25% trypsin after reaching 90% confluence.

2.4.1. Cell viability assay

The Cell Counting Kit-8 (CCK-8) assay was conducted following the guidelines provided by the manufacturer. Briefly, 5 × 10⁴ cells/well were seeded in 24-well plates with different coatings. At the end of the culture, the medium was replaced with 350 μl of basic medium containing 35 μl of CCK-8 solution and incubated for an additional 2 h at 37 °C. Subsequently, transfer the liquid from the 24-well plate to the 96-well plate and the absorbance at 450 nm for each well was measured using an enzyme labeling measuring instrument (Tecan, Infinite 200 Pro, USA).

2.4.2. SEM analysis

The samples of cells were fixed with a 2.5% glutaraldehyde solution at 4 °C for 12 h, followed by dehydration using an ethanol series (15%, 30%, 50%, 70%, 80%, 90%, 95%) in two consecutive 10-min intervals at each concentration. Subsequently, the samples were dehydrated with 100% ethanol in three consecutive 20-min intervals. To preserve the cellular structure, the dried samples were processed using a Leica EM CPD300 and then coated with platinum using an EM ACE600 (60-s deposition, 20 mA). Microstructural characterization was carried out using a scanning electron microscope (WM2017015, HITACHI) operated at 3 kV.

2.4.3. Cell cycle analysis

Cells were seeded on various coatings until reaching 80% confluence. Following trypsin digestion without EDTA, the cells were

collected, gently rinsed, and suspended in ice-cold PBS to ensure a homogeneous cell suspension with minimal aggregation. Subsequently, the cells were centrifuged at 4 °C, 300g for 4 min, and the resulting cell pellet was washed twice with pre-cooled PBS. The washed cells were then stained with a 50 μg/mL propidium iodide (PI) staining solution in the dark for 5 min. Fluorescence emitted by PI was measured using flow cytometry (BD Biosciences, NJ, USA). The proportions of cells in each phase of the cell cycle (G0/G1, S, and G2/M) were analyzed using the dedicated cell cycle analysis software provided with the instrument.

2.4.4. Cell migration test

The Cell migration test was performed using coated-coverslips. Once the cells reached 80% confluence on the respective coatings, scratches of uniform width were created on the cell monolayer using a sterile 200 μl pipette tip. The scratched areas were gently washed three times with PBS. Subsequently, medium without fetal bovine serum (FBS) was added, and the plates were incubated in a 37 °C incubator for 24 h. Microscopic images of the scratches were captured at 0 h and 24 h using a microscope and analyzed using ImageJ software. Each experiment was repeated independently a minimum of three times. The cell migration rate was determined using the following formula:

$$\text{cell migration (\%)} = \left(1 - \frac{\text{width of the scratch at 24 h}}{\text{initial scratch width}} \right) * 100\%$$

2.4.5. Cell attachment and spreading at early stage

Cells were seeded on different coatings (2 cm²) at a density of 4 × 10⁴ cells/cm². At 2 h and 4 h after seeding, the coverslips were gently washed with PBS and subsequently fixed by immersion in 4% paraformaldehyde for 15 min. The coverslips were then treated with PBS containing 0.2% (v/v) Triton X-100 for 10 min, followed by three rinses with PBS. Subsequently, all coverslips were sequentially stained with phalloidin-TRITC (red fluorescent dye, Cas: CA1610, Solarbio) to visualize actin filaments, and DAPI (blue) to stain the cell nuclei. The cell morphology was examined using laser scanning confocal microscopy (LSMC) (Nikon A1, Japan).

2.4.6. Cell adhesion assay

The cell adhesion assay was conducted following previously described methods [40]. In brief, 4 × 10⁴ cells per well were seeded into 24-well plates on coverslips that were pre-coated with 10 μg/mL collagen (Sigma, Cat.No.9007-34-5) as the control, and onto various coatings as treatments. After 4 h of incubation, the plates were gently washed with PBS for 15 min to remove non-adherent cells. The attached cells were subsequently assessed for cell viability using CCK-8. The cell adhesion rate was determined using the following formula:

$$\text{cell adhesion (\%)} = \left(\frac{\text{OD of Adhesion cells}}{\text{OD of Total cells}} \right) * 100\%$$

2.4.7. Intracellular ROS level and fluorescence analysis

Oxidative stress induction in cells was performed using H₂O₂ [41]. Cells were seeded onto coated-coverslips at a density of 5 × 10⁴ cells/cm². After 24 h of culture, the medium was replaced with MEM containing or lacking 500 μM H₂O₂ for 12 h. The negative control was maintained with MEM supplemented with 10% FBS. The ROS level of cells was evaluated using DCFH-DA (Beyotime, China, S0033) following the provided instructions. DCFH-DA was diluted with serum-free medium to a final concentration of 10 μmol/L, and the collected cells were suspended in the diluted DCFH-DA solution, incubating in a cell incubator for 20 min to ensure complete probe-cell contact. Prior to detection using flow cytometry (BD Biosciences, USA), the cells were washed thrice with serum-free cell culture medium to remove any residual DCFH-DA.

2.4.8. Osteogenic differentiation assay

MEM medium containing 100U/ml penicillin, 100mg/ml streptomycin and 10% FBS was supplemented with 10 mM β -glycerol phosphate (Sigma-Aldrich, USA), 0.1 μ M dexamethasone (Sigma-Aldrich, USA), and 0.25 mM ascorbic acid (Sigma-Aldrich, USA) to prepare osteogenic medium. To induce osteogenic differentiation of BMSCs into osteocytes, BMSCs were co-cultured for several days with osteogenic induction medium. Alkaline phosphatase (ALP) activity and alizarin red staining were used as early and late markers of osteogenic differentiation, respectively. BMSCs were seeded at a density of 2×10^4 cells/well. After 7 days of osteogenic induction, ALP activity was evaluated by staining using the BCIP/NBT Alkaline Phosphatase Color Development Kit (Cas: G1481, Beijing Solarbio Science & Technology Co., Ltd.) and ALP Assay Kit (Beyotime, China) according to the manufacturer's instructions. To assess late-stage mineralization, cells were fixed with 4% paraformaldehyde after 14 and 21 days of culture, then were incubated with 0.1% alizarin red S solution (pH 4.2) for 30 minutes. After being observed and photographed with a microscope, calcium deposits were extracted using 10% cetylpyridinium chloride solution for 1 hour and were quantified by measuring absorbance at 593 nm.

2.5. Animal test

Eighteen Sprague-Dawley (SD) rats weighing approximately 300g and aged around 6 weeks were randomly assigned to three groups: control (Ti rods without coating), PC/Fe-MPNs (Ti rods coated with (PC/Fe)₁₀-MPNs), and PC/Fe@c(RGDfc) (Ti rods coated with PC/Fe@c(RGDfc)). After intraperitoneal injection of 1 mL of 10% sodium pentobarbital solution, a 1 cm skin incision was made in the femur of the rear leg to expose the lateral side of the femur. The implants, measuring 1 mm in diameter and 6 mm in length, were inserted perpendicularly into the femurs using constant cooling with 0.9% NaCl solution.

Following disinfection with povidone iodine, the wound was sutured, and cefuroxime sodium was administered via intramuscular injection daily to prevent infection. After an 8-week period, rats were sacrificed, and femur samples were collected. The samples were immersed in 4% paraformaldehyde for further analysis. All animal procedures were conducted in strict accordance with the Guidelines for Care and Use of Laboratory Animals of Wenzhou Institute, University of Chinese Academy of Sciences (WIUCA) and were approved by the Animal Ethics Committee of WIUCA (WIUCAS23020803).

2.5.1. Microfocus computed tomography (Micro-CT)

The femurs containing the implanted materials were subjected to micro-CT scanning using a voltage source of 80 kV, a current of 300 μ A, and a rotational angle of 360° (with a step rotation of 0.6°) and 36 μ m resolution. The region of interest (ROI) located 200 μ m away from the surface of the titanium implants was reconstructed using the associated software (CTAn and CTVol). From this reconstruction, bone volume (BV), total volume (TV) of bone, and trabecular number (Tb. N) were obtained.

2.5.2. Histological analysis

After micro-CT scanning, histological staining and quantitative analysis were conducted to assess osteogenesis and osseointegration on the surfaces of Ti screws. To begin, all samples were fixed with paraformaldehyde, washed with water, dehydrated in ethanol, and clarified in xylene. Subsequently, they were embedded in poly (methyl methacrylate). The embedded blocks were then sectioned into slices measuring 300 μ m in thickness along the longitudinal axis and implantation centre using a hard tissue slicer (EXAKT 300CP). These sections were further ground down to a thickness of 10 μ m using a Grinding System (EXAKT 400 CS). Next, the samples were stained with toluidine blue, and images were captured using an optical microscope (Ni-U, NIKON). The bone-implant contact (BIC), which represents the percentage of the implant circumference directly in contact with bone tissue in the threaded area,

was quantified using Image-Pro Plus6.0 software. The mean BIC (%) was determined using the following formula:

$$\text{mean BIC (\%)} = \left(\frac{\text{contact lengths between bone and implant}}{\text{length of the implant within the bone tissue}} \right) * 100\%$$

2.5.3. Protein isolation and western blot

Total protein was extracted from the tissue surrounding the implants using a RIPA buffer (Beyotime, China, P0013B) supplemented with 1 mmol/l PMSF (Beyotime, China, ST505). Proteins (40 μ g) were separated by SDS-PAGE (6% and 12%) and transferred to PVDF membranes (USA, Millipore, IPVH00010). Following transfer, the membranes were blocked in Tris-buffered saline (TBST) containing 5% nonfat milk at 37 °C for 2 h. Subsequently, they were incubated overnight at 4 °C with primary antibodies against Collagen I (1:750; AF7001, Affinity Biosciences, OH, USA), Vinculin (1:1000; AF5122, Affinity Biosciences, OH, USA), Cyclin (1:1000; AF0931, Affinity Biosciences, OH, USA), and beta-Actin (1:10000; AF7018, Affinity Biosciences, OH, USA). After washing the membranes three times with TBST solution, they were incubated with secondary antibodies (1:6000; S0001, Affinity Biosciences, OH, USA) for 1–2 h at 37 °C. The bands were visualized using an ECL-Plus detection kit (New Cell & Molecular Biotech Co., Ltd, P10100), and the membranes were analyzed using ImageJ software.

2.5.4. Biomechanical push-out test

Bone-implant interfacial shear strength was evaluated by push-out testing. Femur samples containing titanium rod implants were mounted on an Instron E10000 instrument equipped with a 500 N load cell. The titanium rods were pulled out at a constant rate of 1 mm/min until completely detached from the surrounding bone. Maximum load at implant failure was recorded as the interfacial shear strength.

2.6. Data processing and statistical analysis

Statistical analyses were conducted using GraphPad Prism 9.5 (GraphPad Software Inc., CA, USA). The graphs were generated using Origin 2023b (OriginLab, MASS, USA). The results are presented as mean \pm standard deviation (SD). The *t*-test was employed to assess the significant difference between each pair of groups, and was indicated by the symbols "*", "**" and "***" for $p < 0.05$, $p < 0.01$ and $p < 0.001$, respectively. # $p < 0.05$, ## $p < 0.01$ or ### $p < 0.001$ indicated a statistically significant difference compared to the Control group. No significance was noted as "ns". Independent replication of all experiments was performed three times, unless otherwise specified.

3. Results and discussion

3.1. Preparation and characterization of PC/Fe@c(RGDfc)

The PC/Fe@c(RGDfc) hybrid coating composed of a (PC/Fe)₅-MPNs complex layer with an average thickness of 32.08 ± 1.43 nm (Fig. S1) and a following conjugated c(RGDfc) peptide layer with an average thickness of 12.15 ± 1.24 nm (Fig. 1a). The presence of peaks corresponding to characteristic elemental signals (such as S2p and N1s in c(RGDfc)) in the XPS spectra directly confirmed the success of the c(RGDfc) modification (Fig. 1b), which could be supported by the changed elements (S, N, Fe, O, and C) in the PC/Fe-MPNs and PC/Fe@c(RGDfc) (Fig. 1c). The ratio of S and N elements on the PC/Fe@c(RGDfc) coating surface is (1.12:8.98), which is approximately equal to the ratio of S and N elements in c(RGDfc) (C₂₄N₈O₇S₁), which also indicates that c(RGDfc) peptide was nondestructively grafted on the PC/Fe-MPNs surface.

The grafting of c(RGDfc) can alter surface charge and hydrophilicity. Zeta potential measurements of (PC/Fe)₅-MPNs and PC/Fe@c(RGDfc) coatings on PS spheres showed that (PC/Fe)₅-MPNs had a negative surface charge, while the PC/Fe@c(RGDfc) composite coatings had

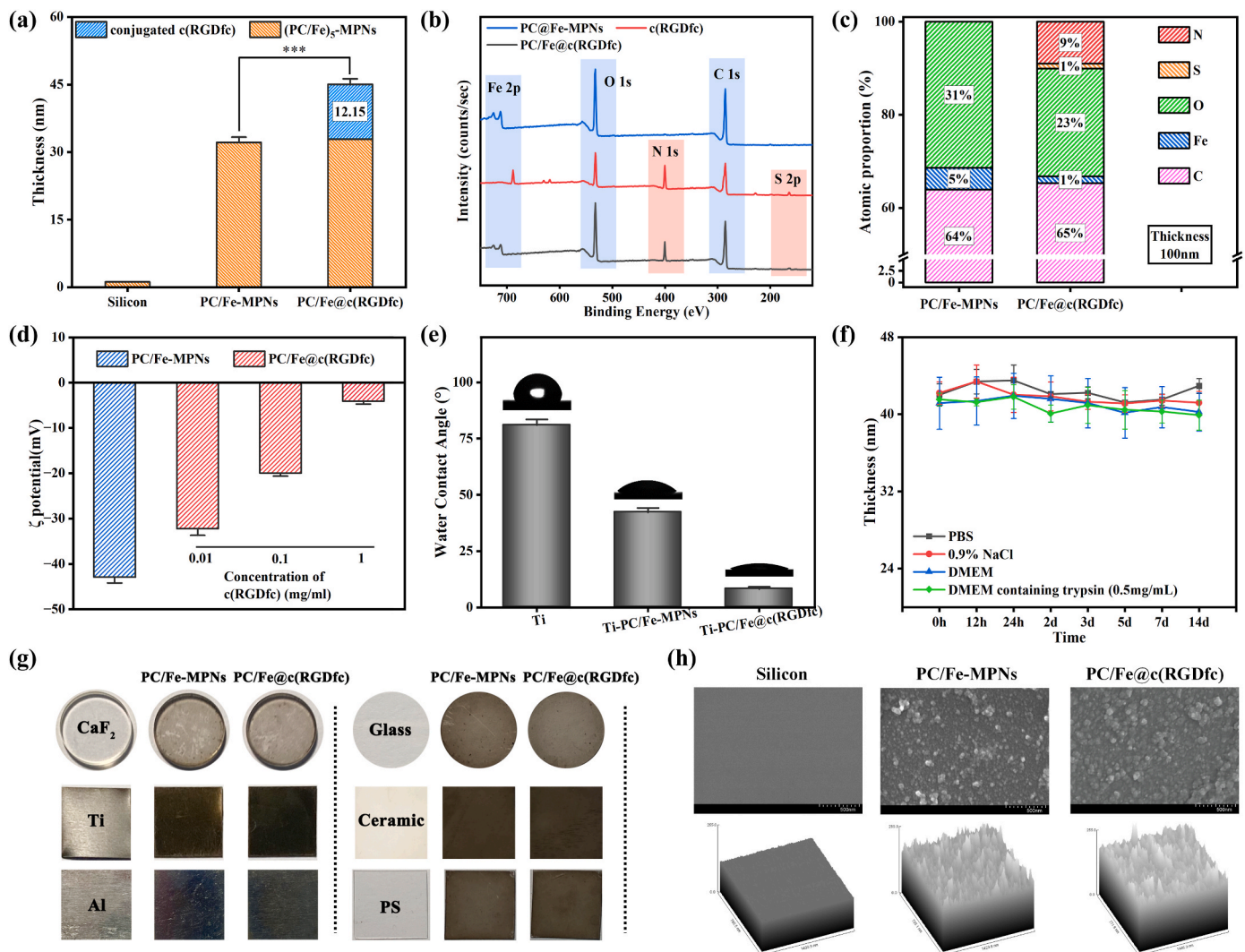


Fig. 1. Characterization of PC/Fe@c(RGDfc). (a) The thickness of c(RGDfc) adsorbed on (PC/Fe)₅-MPNs. (b) The total XPS spectra of the PC/Fe-MPNs and the PC/Fe@c(RGDfc) coatings, along with the elemental molar ratio obtained by XPS analysis in (c). (d) Zeta potential changes of coating surface resulting from c(RGDfc) adsorption at different concentrations on (PC/Fe)₅-MPNs, while surface hydrophilicity changes of both types of composite coatings are shown in (e). (f) The variation of coating thickness with treatment time in PBS, 0.9%NaCl, DEME with or without 0.25% trypsin. (g) Optical photographs of PC/Fe-MPNs and PC/Fe@c(RGDfc) composite coatings on different substrates. (h) SEM photos and ImageJ roughness fitting of these coatings adhering to silicon substrate. N = 3, no significance noted as "ns," *p < 0.05, **p < 0.01, ***p < 0.001, using *t*-test. (For interpretation of the references to color in this figure legend, the reader is referred to the Web version of this article.)

significantly increased surface charge with increasing c(RGDfc) concentration (Fig. 1d). Additionally, c(RGDfc) grafting altered surface hydrophilicity. The introduction of hydrophilic PC/Fe complexes resulted a lower water-contact angle for the Ti surface. Modification with c(RGDfc) peptides further decrease water-contact angle, resulting in a super-hydrophilic PC/Fe@c(RGDfc) composite coating (Fig. 1e). As a composite coating with the potential to promote organization and integration and repair, it must maintain good stability under physiological conditions. Coatings were evaluated for stability by immersion in PBS, 0.9% NaCl solution, DMEM medium, and DMEM containing trypsin (0.5 mg/mL), and changes in thickness were monitored over time (Fig. 1f). Results showed that the coating thickness did not significantly decrease during the 14 days observation period, indicating the PC/Fe@c(RGDfc) composite coating remained stable.

The PC/Fe-MPNs coating and PC/Fe@c(RGDfc) coating were synthesized on various types of substrates (Fig. 1g). Obvious black coating attachment could be observed on the surface of CaF₂, Ti, Al, Glass, Ceramic and PS. Since c(RGDfc) is a colorless and transparent material, there is no significant difference between PC/Fe-MPNs coating and PC/

Fe@c(RGDfc) coating under the light microscope. Further, surface morphology was observed using scanning electron microscopy (SEM) (Fig. 1h). Compared with the unmodified Silicon surface, the deposition of PC/Fe complexes leads to the aggregation of nanoparticles, resulting in an increase in surface roughness of PC/Fe-MPNs. Further fixation of c(RGDfc) resulted in an increase in coating thickness but had no significant effect on its structural features and surface roughness.

3.2. Mechanism and Factors of constructing PC/Fe@c(RGDfc)

X-ray Photoelectron Spectroscopy (XPS) and Liquid Chromatography-Mass Spectrometry (LC-MS) was used to reveal the main mechanism of PC/Fe@c(RGDfc) construction. In the detailed C1s spectra of the PC/Fe-MPNs (Fig. S2b), three peaks were observed: C–C/C=C at 284.3 eV [36], C–O at 286.4 eV [42] and C=O at 288.1 eV [43]. In contrast to the C1s spectra of PC (Fig. S2a), the presence of C=O bond at 288.1 eV suggests that under alkaline conditions (pH = 8.5, in air), the remaining hydroxyl group on PC was oxidized to form a semi-quinone radical under the action of oxygen, which subsequently rearranged to

quinones [44,45]. It has been reported that such oxidation often occurs in the B ring (catechol or galloyl group) of flavonoid polyphenols with C6–C3–C6 structure [46]. These reactive intermediate products readily react with cysteinyl thiol group in c(RGDfc) [47].

To investigate whether physisorption was involved in the formation of the PC/Fe@c(RGDfc) coating, PC/Fe@c(RGDfc) was immersed in 2% Sodium dodecyl sulfate (SDS) solution with gentle shaking for 10 min to elute possible physisorption c(RGDfc) layer [48]. The results in Fig. S3 show that compared with the thickness before washing (40.04 ± 1.57), the thickness after washing (39.88 ± 1.20) did not decrease significantly. This completely excludes the formation of a c(RGDfc) layer on the PC/Fe-MPNs coating surface due to physical adsorption. Meanwhile, in the detailed N1s spectra of c(RGDfc) and PC/Fe@c(RGDfc)

coatings (Fig. 2a and b), the peak area ratio of C=N bond (8.94%–9.52%) did not change. On the other hand, the ratio of C=N and C=O in the C1s spectrum of PC/Fe@c(RGDfc) is maintained at 2.16: 15.75 (Fig. S2c). Both of these suggest that the arginine residue of c(RGDfc) did not react, implying that the Schiff base bond was not involved in the grafting of c(RGDfc). Therefore, we considered that the covalent binding of free PC residues on the PC/Fe-MPNs coating to the c(RGDfc) cysteine residue resulted in the grafting of c(RGDfc) peptide, for which we examined the interaction between PC and c(RGDfc) peptide by LC-MS. As shown in Fig. 2c, the analysis of intact c(RGDfc) revealed a peak at 579.2 *m/z*. When c(RGDfc) (1 mM) was incubated with PC (1 mM) in 10 mM Tris-HCl buffer (pH 8.5) at 37 °C for 30 min, the intensity of the c(RGDfc) peak was reduced. Meanwhile, since the modified c(RGDfc)

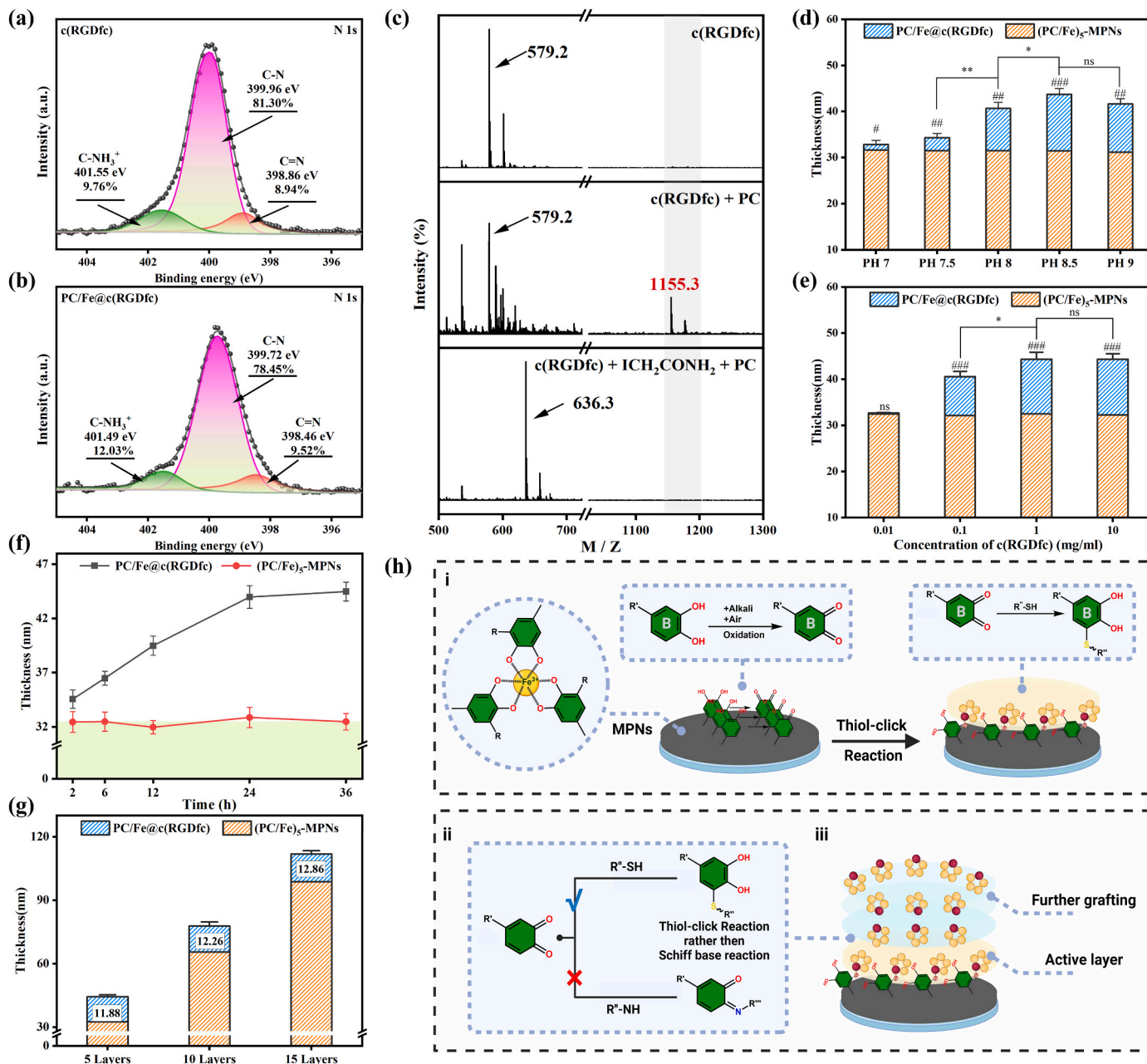


Fig. 2. Mechanism and Factors of the construction of c(RGDfc) peptide-grafted PC/Fe-MPNs substrates. N1s peaks of (a) c(RGDfc) and (b) the PC/Fe@c(RGDfc) composite coating. (c) LC-MS analysis of the interaction between c(RGDfc) and PC. (d) The thickness of c(RGDfc) adsorbed on (PC/Fe)₅-MPNs at different pH values, (e) concentrations of c(RGDfc), and (f) after different deposition time. (g) Thickness changes of c(RGDfc) grafted on PC/Fe-MPNs fabricated with different cycles in the PC/Fe-MPNs fabrication process. (h) Schematic of the PC/Fe@c(RGDfc) coating construction mechanism, Created with BioRender.com. N = 3, no significance noted as "ns," *p < 0.05, **p < 0.01, ***p < 0.001, and #p < 0.05, ##p < 0.01 or ###p < 0.001 compared with the Control group, using t-test.

corresponds to the addition of one molecule of PC per peptide, a peak of 1155.3 m/z was generated. On the other hand, no adduct peak was observed after incubation of thiol-alkylated (S-carbamidomethylated) c(RGDfc) (636.3 m/z) and PC, indicating that the cysteine thiol group is the target of covalent modification of PC. These observations provide strong evidence that c(RGDfc) can covalently bind PC via the sulfhydryl group in cysteine, generating S-cysteinyl-PC conjugates, which resulted in grafting of c(RGDfc) onto PC/Fe-MPNs coating.

With the judgement on coating thickness tested by optical ellipsometry, and the coating conditions were optimized by varying the pH (Fig. 2d), concentration of c(RGDfc) solution (Fig. 2c), and deposition time (Fig. 2f). When the c(RGDfc) concentration was maintained at 1 mg/mL in a buffer with a pH value of 8.5, the thickness growth of the PC/Fe@c(RGDfc) coating reached equilibrium within 24 h, at about 44.57 ± 1.048 nm. However, the results in Fig. 2f show that the grafting of c(RGDfc) on the surface of PC/Fe-MPNs was a slow process, which is not consistent with the rapid grafting rate of thiol-click reaction [49]. Meanwhile, the growth of the grafting thickness (12.15 ± 1.24 nm) is much higher than the monolayer thickness of c(RGDfc). And the results in Fig. 2g showed that when the number of deposition layers of PC/Fe-MPNs was 5, 10 and 15, the thickness of c(RGDfc) grafting was measured to be 11.88, 12.26 and 12.86 nm, which also means that

substrate thickness of substrates had no discernible effect on the grafting of c(RGDfc). Based on this result, it's not hard to speculate the presence of active layer of PC/Fe-MPNs, which is conducive to the further grafting of c(RGDfc) peptide. Beneath the active growth layer, the inert layer cannot react with c(RGDfc) peptide might because it's difficult to be reachable by the diffusing c(RGDfc).

Based on the experimental results, we can summarize the following key principles underlying the c(RGDfc) grafting process onto the surface of PC/Fe-MPNs (Fig. 2h): i. In a weak alkaline solution environment, oxidative reactions occur on the phenolic hydroxyl groups of PC residues, generating quinone intermediates. These quinones then react further with the sulfhydryl groups of c(RGDfc), enabling the grafting of c(RGDfc) onto the PC/Fe-MPNs surface. This process does not damage the RGD residues. ii. The grafting of c(RGDfc) onto the PC/Fe-MPNs surface is dominated by Thiol-click reactions rather than Schiff base reactions. iii. The presence of an activation layer on the surface of PC/Fe@c(RGDfc) results in a thicker grafting of the c(RGDfc).

3.3. Mechanical properties of different surfaces

Atomic force microscopy (AFM) was used to investigate the mechanical properties of different bioactive coatings in both air and liquid

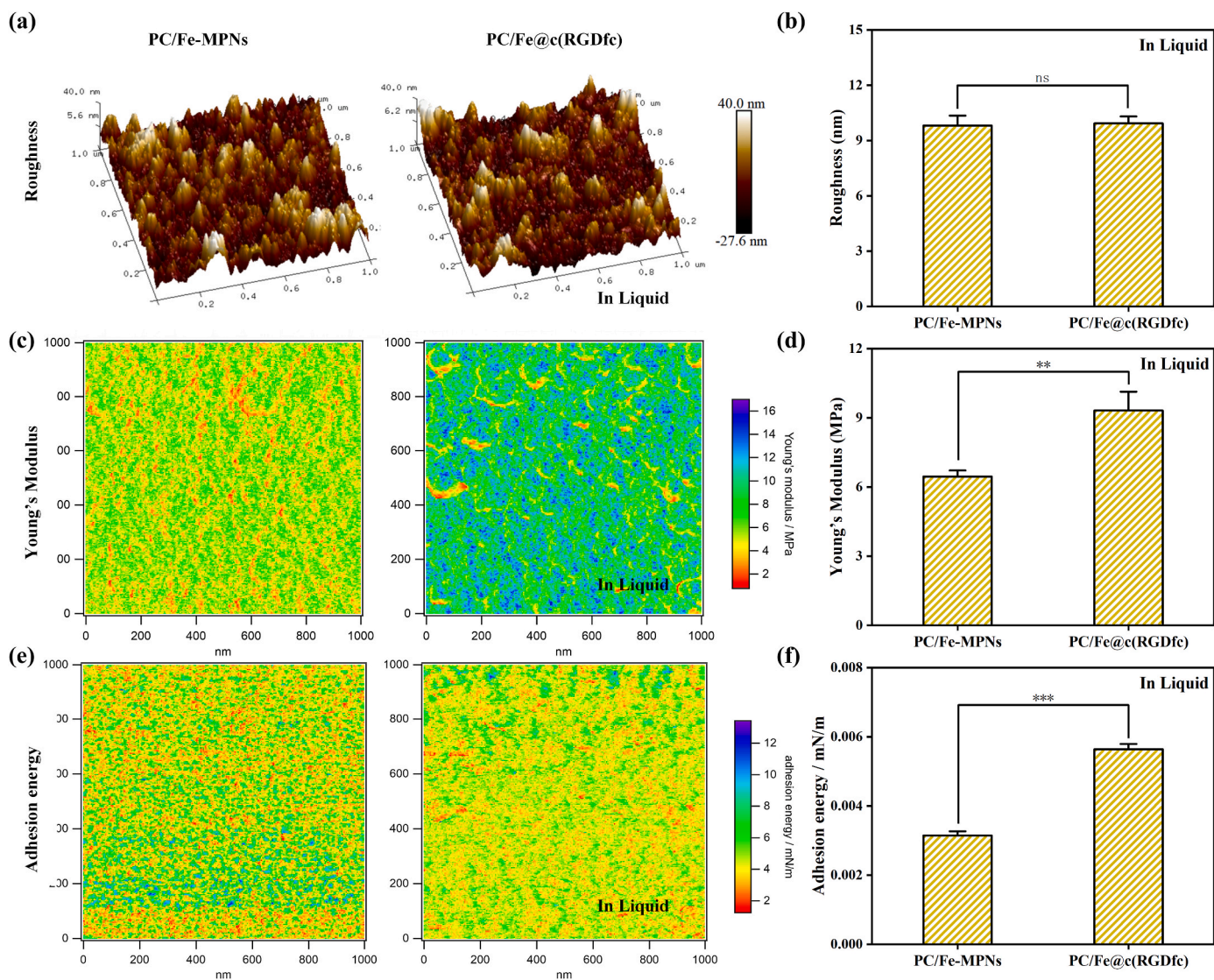


Fig. 3. AFM images of PC/Fe-MPNs and PC/Fe@c(RGDfc) coatings in Liquid environment. (a–b) Surface roughness, (c–d) Young's modulus images and (e–f) Adhesion energy representative images and quantitative analysis. N = 3, no significance noted as "ns," * $p < 0.05$, ** $p < 0.01$, *** $p < 0.001$, using t -test.

phases. The surface morphology, young's modulus and adhesion energy of the coatings was analyzed using Nano Scope analysis software. As demonstrated in Fig. 3a and Fig. S4a. In the air phase, the PC/Fe@c(RGDfc) coating had lower roughness compared to PC/Fe-MPNs coating (Fig. S4b), which could be attributed to the presence of grafted c(RGDfc) peptide. In the liquid phase, the roughness of the PC/Fe@c(RGDfc) coating was almost the same as that of PC/Fe-MPNs, with the former being 9.93 ± 0.378 nm and the latter being 9.81 ± 0.541 nm (Fig. 3b). The increased roughness of the PC/Fe@c(RGDfc) coating in the liquid phase may be attributed to the hydration and extension of the peptide molecules on the coating surface [50]. The Young's modulus of the PC/Fe@c(RGDfc) coating was higher than that of PC/Fe-MPNs in the liquid environment (Fig. 3c and d), which was consistent with that observed in the air (Figs. S4c and d). The adhesion of the coating surface was obtained using the JKR theoretical equation. The result showed that

the adhesion energy of PC/Fe@c(RGDfc) coating was found to be higher than that of the PC/Fe-MPNs coating in both air (Figs. S4e and f) and liquid (Fig. 3e and f) environments. Overall, these results indicate that the grafting of the c(RGDfc) peptide can alter the mechanical properties of PC/Fe-MPNs coating, and the better mechanical properties suggest potential applications in biology.

3.4. Cell proliferation and migration ability of different surfaces

The essential capabilities inherent to cells, such as proliferation [51], adhesion [52] and migration [53], are considered to be important aspects of cell biology research. These basic functions directly exert direct influence on diverse aspects, including cell growth, differentiation, repair, immune response, ultimately orchestrating the intricate interplay involved with regenerating local tissue deficits and facilitating

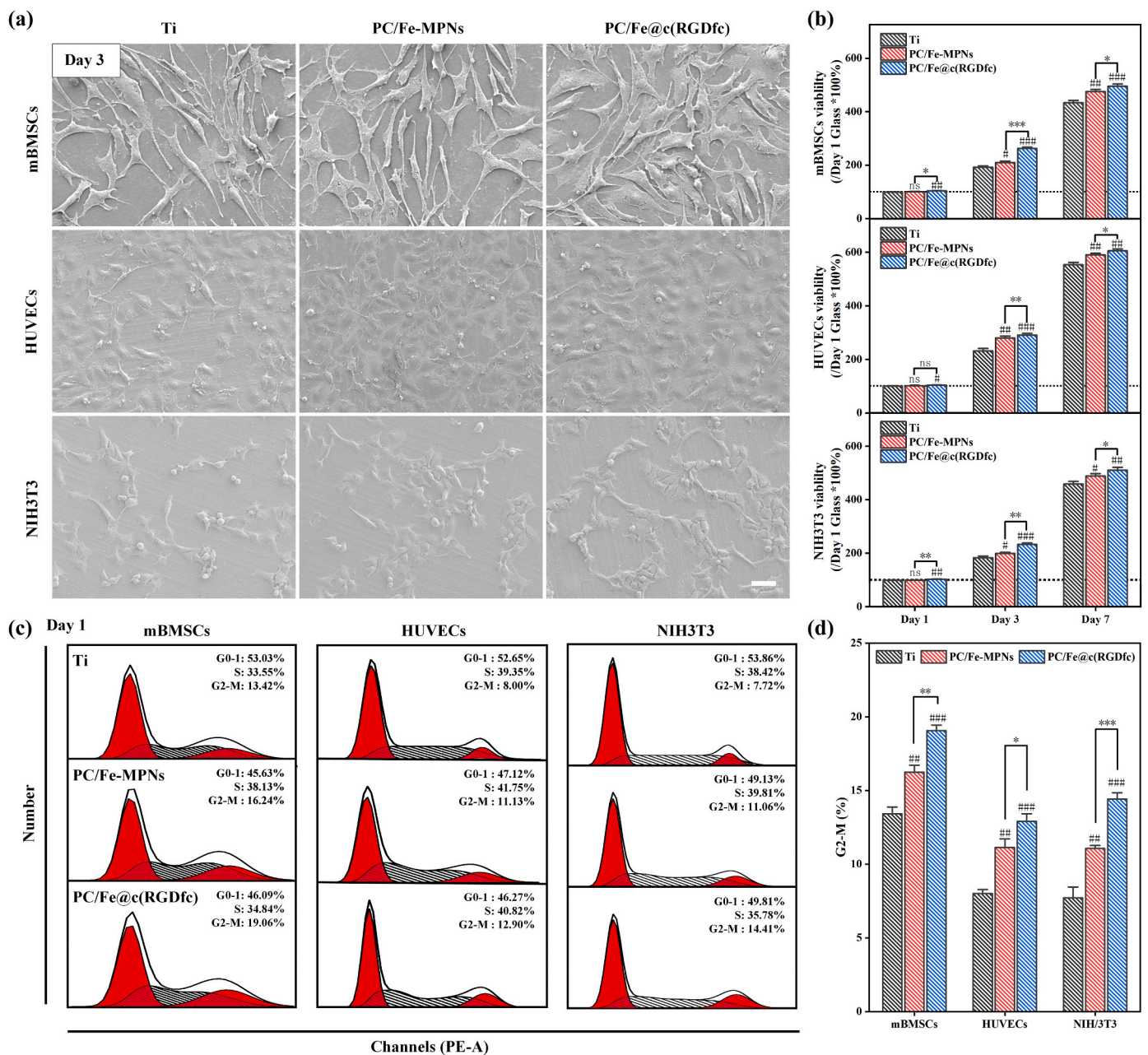


Fig. 4. SEM images (a) and cell viability (b) of mBMSCs, HUVECs and NIH3T3 cultured on Ti, Ti-PC/Fe-MPNs, and Ti-PC/Fe@c(RGDfc). Cell cycle experiments in different cells on Ti, Ti-PC/Fe-MPNs, and Ti-PC/Fe@c(RGDfc). Scale bars in (a) are 200 nm. N = 3, no significance noted as "ns," *p < 0.05, **p < 0.01, ***p < 0.001, and #p < 0.05, ##p < 0.01 or ###p < 0.001 compared with the Control group, using t-test.

tissue integration [54]. Moreover, diverse cell types partake in the intricate process of tissue repair. For example, in the context of bone defect restoration, stem cells, osteoblasts, chondrocytes, vascular endothelial cells, fibroblasts, and immune cells all play critical roles. Therefore, in this study, three distinct cell types, including mouse bone marrow mesenchymal stem cells (mBMSCs), human umbilical vein endothelial cells (HUVECs), and a mouse fibroblast cell line (NIH3T3), were selected and inoculated onto the surface of Ti, glass, and other substrates to simulate cell process on bone implant surfaces and investigate the effect of PC/Fe@c(RGDfc) composite coating.

Following onset of disease and tissue damage, cellular proliferate is necessary to replenish the loss of damaged cells [51]. SEM images (Fig. 4a) showed a significant increase in the number of cells on the surfaces of Ti-PC/Fe-MPNs and Ti-PC/Fe@c(RGDfc) after three days of culture, surpassing those observed on bare Ti surfaces. Furthermore, the PC/Fe@c(RGDfc) composite coatings had a higher cellular density with

fuller cell morphology. Meanwhile, the cell viability was measured by CCK-8 (Fig. 4b), and the results showed that the cell viability of cells cultured on the Ti-PC/Fe@c(RGDfc) surface was significantly better than that on Ti and Ti-PC/Fe-MPNs. Notably, this difference peaks at day three, gradually diminishing by day seven. After being cultured on different substrates for 1 day, the proportion of each phase in the cell cycle of the three cell lines is shown in Fig. 4c, while Fig. 4d shows that the proportion of cells in G2-M phase was significantly higher on PC/Fe-MPNs and PC/Fe@c(RGDfc) composite coatings than on the Ti surface. The effect of PC/Fe@c(RGDfc) composite coating is more specific than that of PC/Fe-MPNs coating. This indicated that cells on PC/Fe@c(RGDfc) composite coatings entered the cell division cycle (M phase) earlier and exhibited stronger cell proliferative activity.

During the process of tissue injury repair, cell migration is one of the key steps in restoring the function of the damaged site. Various types of cells such as fibroblasts, stem cells, and endothelial cells need to migrate

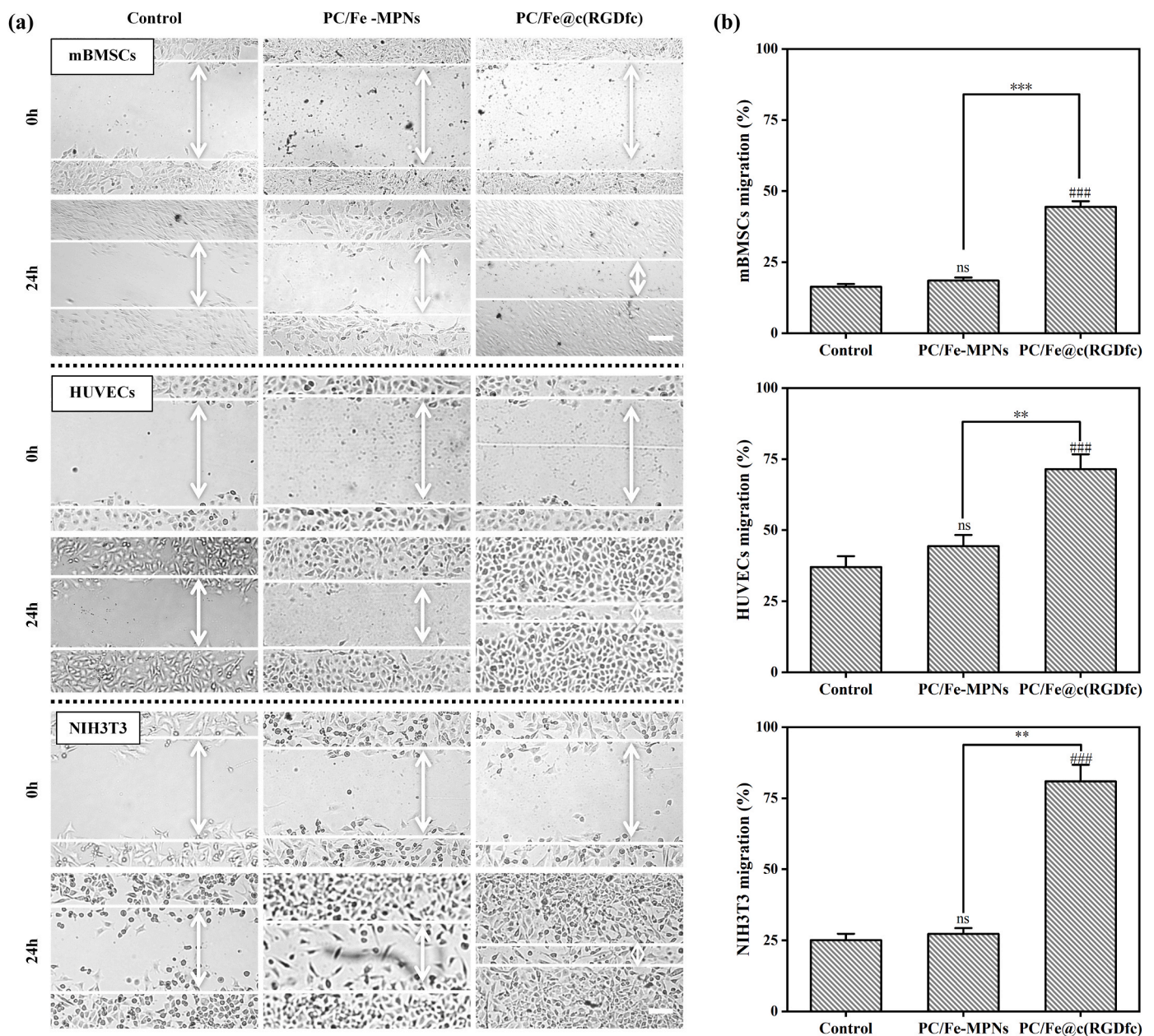


Fig. 5. (a) Scratch test of mBMSCs, HUVECs and NIH3T3 cultured on Glass, PC/Fe-MPNs, and PC/Fe@c(RGDfc) under serum-free treatment with cell migration rate statistics (b). Scale bars in (a) are 100 μ m. N = 3, no significance noted as "ns," *p < 0.05, **p < 0.01, ***p < 0.001, and #p < 0.05, ##p < 0.01 or ###p < 0.001 compared with the Control group, using *t*-test.

and specifically locate to the injured area to participate in tissue regeneration and repair [51]. Cell migration ability under serum-free culture conditions was observed using a scratch assay. Multiple cells exhibited good crawling ability on the surface of PC/Fe@c(RGDfc) composite coating and almost completely covered the exposed surface after 24 h (Fig. 5a). Quantitative results showed that compared to the glass surface, there was no significant difference in cell migration rate on the PC/Fe-MPNs coating, while cells on the PC/Fe@c(RGDfc) composite coating displayed obvious migration phenomenon (Fig. 5b). These results indicate that the PC/Fe@c(RGDfc) composite coating facilitates directed cell movement.

3.5. Cell-anchoring and antioxidant ability of different surfaces

Quick cell attachment and spreading onto implants at an early stage are beneficial for integrating tissue cells [55]. Cell attachment onto the PC/Fe-MPNs and PC/Fe@c(RGDfc) coatings at an early stage was observed by observing the behavior of three cell lines at 2 h and 4 h after seeding by fluorescent images, and the cells seeded on glass were used as the control. Fig. 6a shows that at 2 h, cells on the surfaces of PC/Fe-MPNs and PC/Fe@c(RGDfc) coatings were lightly dispersed with clear morphology, while cells on the surface of glass were rounded. At 4 h, cells on the surface of PC/Fe@c(RGDfc) coating showed cell fusion, while the cells on glass were slightly spread at 4 h. In a further analysis, the cell area per square millimeter, which is one of the most important

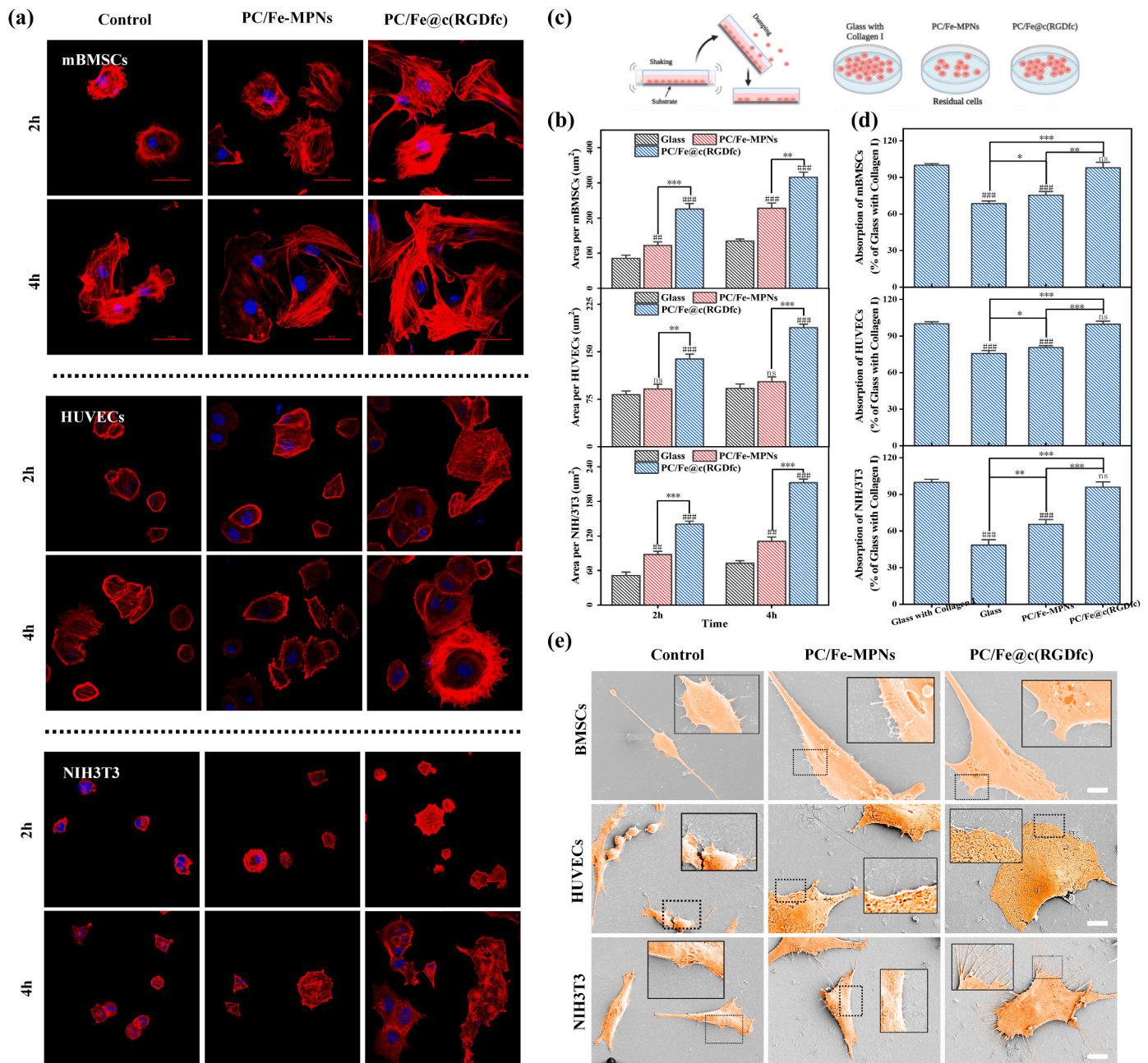


Fig. 6. Adhesion of mBMSCs, HUVECs and NIH3T3 to Glass, PC/Fe-MPNs, and PC/Fe@c(RGDfc) coated substrates. (a) Fluorescence microscopy images of cells seeded on different surfaces for 2 and 4 h. (b) Cell number per square micrometer of the seeded cells. (c) Schematic representation of the cell-substrate adhesion ability assay after cell spreading. (d) Cell-substrate adhesion ability of cells seeded on different surfaces. (e) Cell morphology after attachment of cells to different substrates. Scale bars in (a) are 50 μm, and in (e) are 40 μm. N = 3, no significance noted as "ns," *p < 0.05, **p < 0.01, ***p < 0.001, and #p < 0.05, ##p < 0.01 or ###p < 0.001 compared with the Control group, using t-test.

indices for evaluating attachment at early stage, was also quantified. Fig. 6b showed that the average cell spreading area increased at 4 h for all samples compared to 2 h. Significantly, the adhesion area of cells on PC/Fe@c(RGDfc) coating was larger than that on glass and PC/Fe-MPNs coatings at both 2 and 4 h. In addition, to compare the ability of cells to attach after fully spreading on different surfaces. Cells were inoculated on the surface of Glass, PC/Fe-MPNs, and PC/Fe@c(RGDfc) coatings as shown in Fig. 6c, and the cells seeded on glass with collagen I treatment were used as the control. Eight hours after cell seeding, non-adherent cells were removed using shear force generated by shaking the medium with a horizontal shaker and the residual cell viability was measured by CCK8 to assess the ability of cells to attach after spreading. Fig. 6d results showed that the adhesion ability of cells on PC/Fe@c(RGDfc) coating was significantly different from that of glass or PC/Fe-MPNs coatings and similar to that of collagen I treated glass.

Cell morphology after complete spreading was observed by SEM to evaluate the adhesion ability of cells on Ti implants. Fig. 6e shows that the morphology of cells seeded on the bare Ti surface showed obvious shrinkage of cytoplasm, small volume and obvious nucleus. However, the cells coated with Ti-PC/Fe-MPNs and Ti-PC/Fe@c(RGDfc) still maintained full cell morphology, and the nucleus could not be identified on the cell membrane surface. The cell spreading area of the PC/Fe@c(RGDfc) coated surface cells under the same magnification was also significantly higher than that of Ti and Ti-PC/Fe-MPNs surface cells. Notably, cells on the Ti-PC/Fe@c(RGDfc)-coated surface showed prominent lamellar pseudopods and filamentous pseudopods in contact with the substrate, which facilitated cell attachment and movement on the substrate. The above results indicate that the PC/Fe@c(RGDfc) coating provides a good functional interface for the rapid attachment and dispersion of cells on a variety of material surfaces. The rapid attachment and dispersal of cells onto grafts facilitate their counteraction against the effects of oxidative stress and the inflammatory environment in the early stages of tissue damage repair [56].

The inflammatory response and cell death caused by tissue defect

release excessive free radicals, which often lead to oxidative stress in cells, and oxidative stress can affect cell metabolism and signal transmission, inhibit cell function, and ultimately affect the repair of tissue defects [57]. Hence, it becomes imperative for ideal materials to possess formidable free radical scavenging prowess while concurrently diminishing intracellular reactive oxygen species (ROS) levels. The antioxidant capacity and free radical scavenging capacity of glass, PC/Fe-MPNs and PC/Fe@c(RGDfc) composite coatings were explored by Total Antioxidant Capacity Assay Kit with FRAP method, DPPH Free Radical Scavenging Capacity Assay Kit and ABTS Free Radical Scavenging Capacity Assay Kit. The results of Figs. S5a–d show that compared with the glass, the PC/Fe-MPNs and PC/Fe@c(RGDfc) composite coatings have better total antioxidant and free radical scavenging capacity, and there is no significant difference in the effect between the two coatings. And, the long-term retention of antioxidant and free radical scavenging capacity of PC/Fe-MPNs and PC/Fe@c(RGDfc) composite coatings is significantly higher than VC or Trolox solution. In general, PC/Fe@c(RGDfc) coating provides an ideal antioxidant material for removing excess free radicals around tissues, improving cellular oxidative stress, and enhancing cellular functions.

To investigate the anti-oxidative stress properties of PC/Fe@c(RGDfc) composite coatings, cells cultured on different substrates were treated with hydrogen peroxide, a ROS inducer, to promote intracellular ROS production. Flow cytometry was subsequently applied to measure the levels of intracellular ROS. As depicted in Fig. 7a and b, the anti-oxidative stress effects of PC/Fe@c(RGDfc) are notably evident. ROS plays an important role in intracellular signal transduction and some key physiological responses. However, excessive accumulation of ROS activates the inflammasome, leading to cell damage and death [58]. Proanthocyanidins (PC) have garnered substantial attention for their explicit antioxidant activity, substantiated by copious reports [59]. The newly developed PC/Fe@c(RGDfc) composite coating effectively retained the antioxidant activity of PC, and showed a significant ability to inhibit the overproduction of ROS and the overactivation of

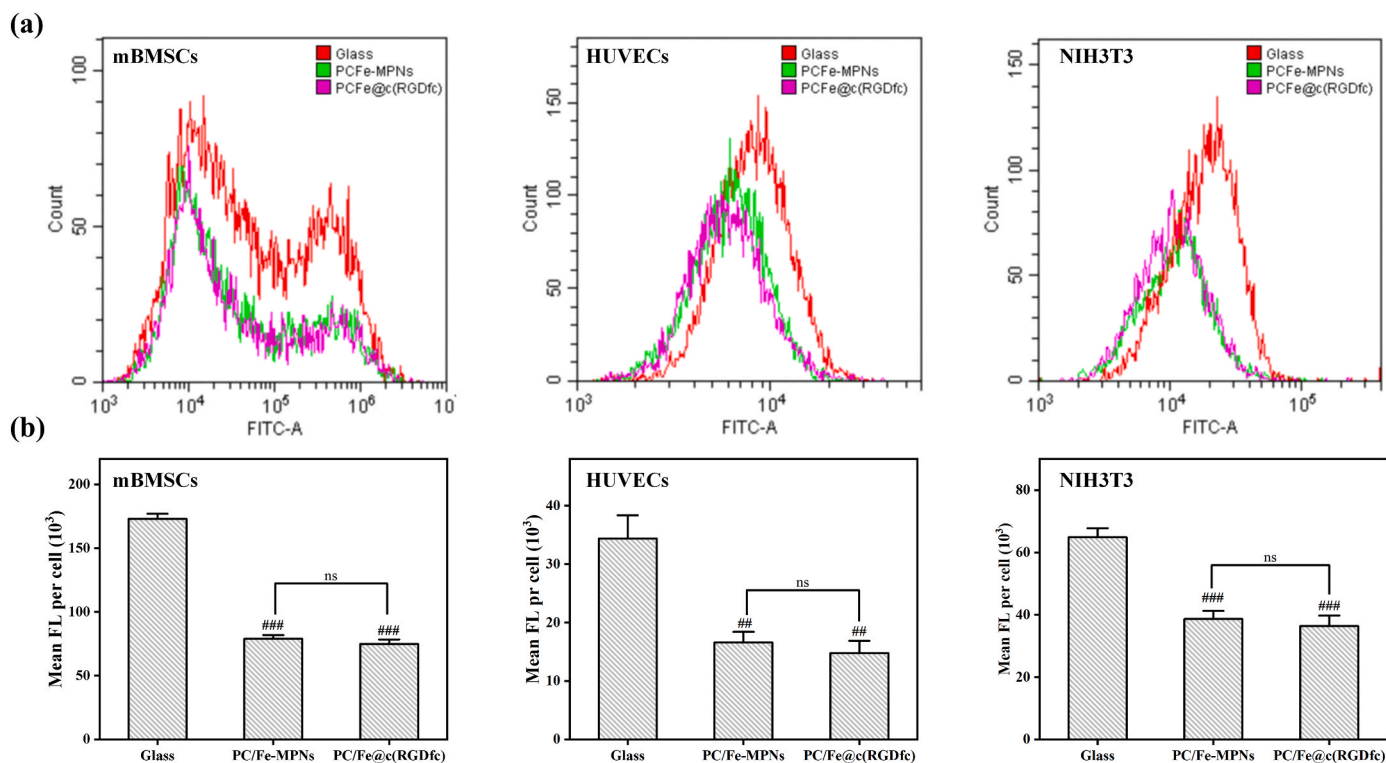


Fig. 7. The intracellular ROS level of different cells cultured in coated or uncoated glass with or without treatment of H_2O_2 was detected by fluorescent staining. (a) The average fluorescence intensity of cells was detected by flow cytometry. (b) Comparison of data from (a). N = 3, no significance noted as "ns," * $p < 0.05$, ** $p < 0.01$, *** $p < 0.001$, and # $p < 0.05$, ## $p < 0.01$ or ### $p < 0.001$ compared with the Control group, using t-test.

ROS-related signaling pathways during tissue damage repair. Improvement of the oxidative stress microenvironment will significantly affect cell function, thereby improving implant-tissue integration [60]. Consequently, this material, endowed with exceptional free radical scavenging capabilities, holds immense potential in enhancing cellular function and facilitating tissue regeneration.

3.6. Osteointegration ability of PC/Fe@c(RGDfc) in vitro and in vivo

In order to explore the in vitro osteogenic ability of PC/Fe@c(RGDfc) coating, we inoculated mBMSCs on the surfaces of coated or uncoated PC/Fe-MPNs and PC/Fe@c(RGDfc) coating. After 3 days and 7 days of osteogenic induction culture, alkaline phosphatase (ALP) staining of MC3T3-E1 cells on the coating surface was shown in Fig. 8a. The ALP activity analysis in Fig. 8b further proved that, whether at 3 days or 7 days, the ALP activity of mBMSCs cells in the PC/Fe@c(RGDfc) coating group was significantly stronger than that in the Control and the PC/Fe-MPNs coating group, indicating that the peptide-containing coating enhanced early osteogenesis. After 14 days and 21 days of osteogenic

induction culture, alizarin red staining (ARS) and calcium quantification of mBMSCs cells were shown in Fig. 8c and d respectively. The results showed that the calcium content of PC/Fe@c(RGDfc) group was significantly higher than that of Control and PC/Fe-MPNs groups at either 3 or 7 days, suggesting that PC/Fe@c(RGDfc) coating significantly promoted the osteogenic mineralization ability of mBMSCs.

To further ascertain the in vivo osseointegration efficacy of the PC/Fe@c(RGDfc) coating, which possesses antioxidant, osteogenic and cell-regulatory capabilities, we surgically implanted Ti rods, with and without the aforementioned coating, into rat models exhibiting bone defects within corresponding regions of the femur for 8 weeks (Fig. S6). Micro-CT results showed that the Ti-(PC/Fe)₁₀@c(RGDfc) implant group had significantly higher BV/TV (bone volume/tissue volume %) and trabecular number (Tb. N 1/mm) compared with the Ti and Ti-(PC/Fe)₁₀-MPNs groups, suggesting that the Ti-(PC/Fe)₁₀@c(RGDfc)-coated material has an osteogenesis-promoting effect in vivo (Fig. 9a-d). Morphological analysis of histological staining and bone-implant contact (BIC) are the most direct evidence for evaluating osseointegration. As shown in Fig. 9e, Ti-(PC/Fe)₁₀@c(RGDfc) had the best bone

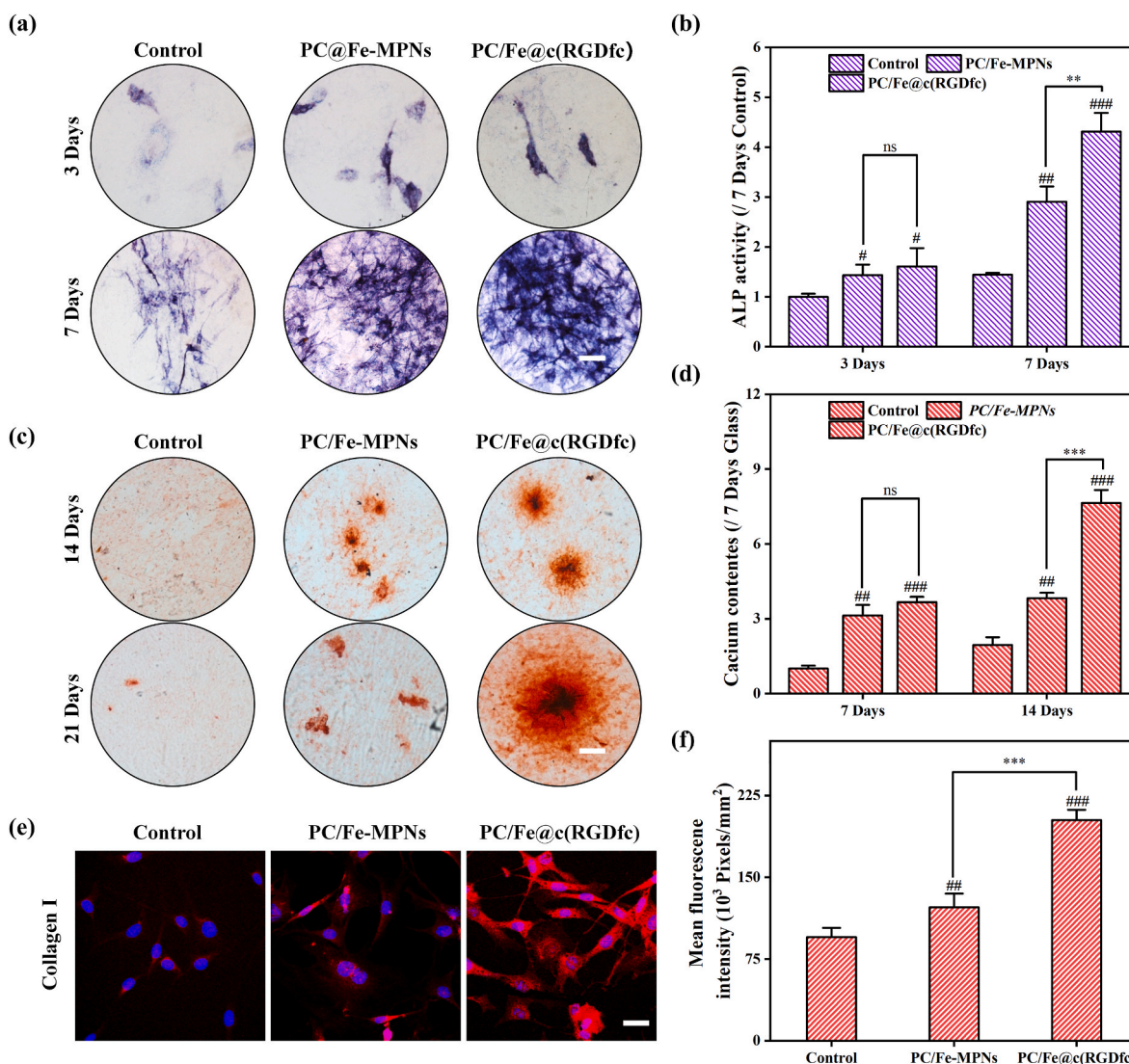


Fig. 8. PC/Fe@c(RGDfc) coating promoted cell osteogenesis in vitro. Representative images of ALP staining of mBMSCs cultured on different coatings on days 3 and 7 of cell culture (a) and detection of ALP activity (b). Representative images of ARS staining (c) and quantification of calcium nodules (d) of mBMSCs cultured on different substrates for 7 d, and nuclei (blue) and collagen I (red) staining were performed. N = 3, no significance noted as "ns", ***p < 0.001 using *t*-test. N = 3, no significance noted as "ns", *p < 0.05, **p < 0.01, ***p < 0.001, and #p < 0.05, ##p < 0.01 or ###p < 0.001 compared with the Control group, using *t*-test. (For interpretation of the references to color in this figure legend, the reader is referred to the Web version of this article.)

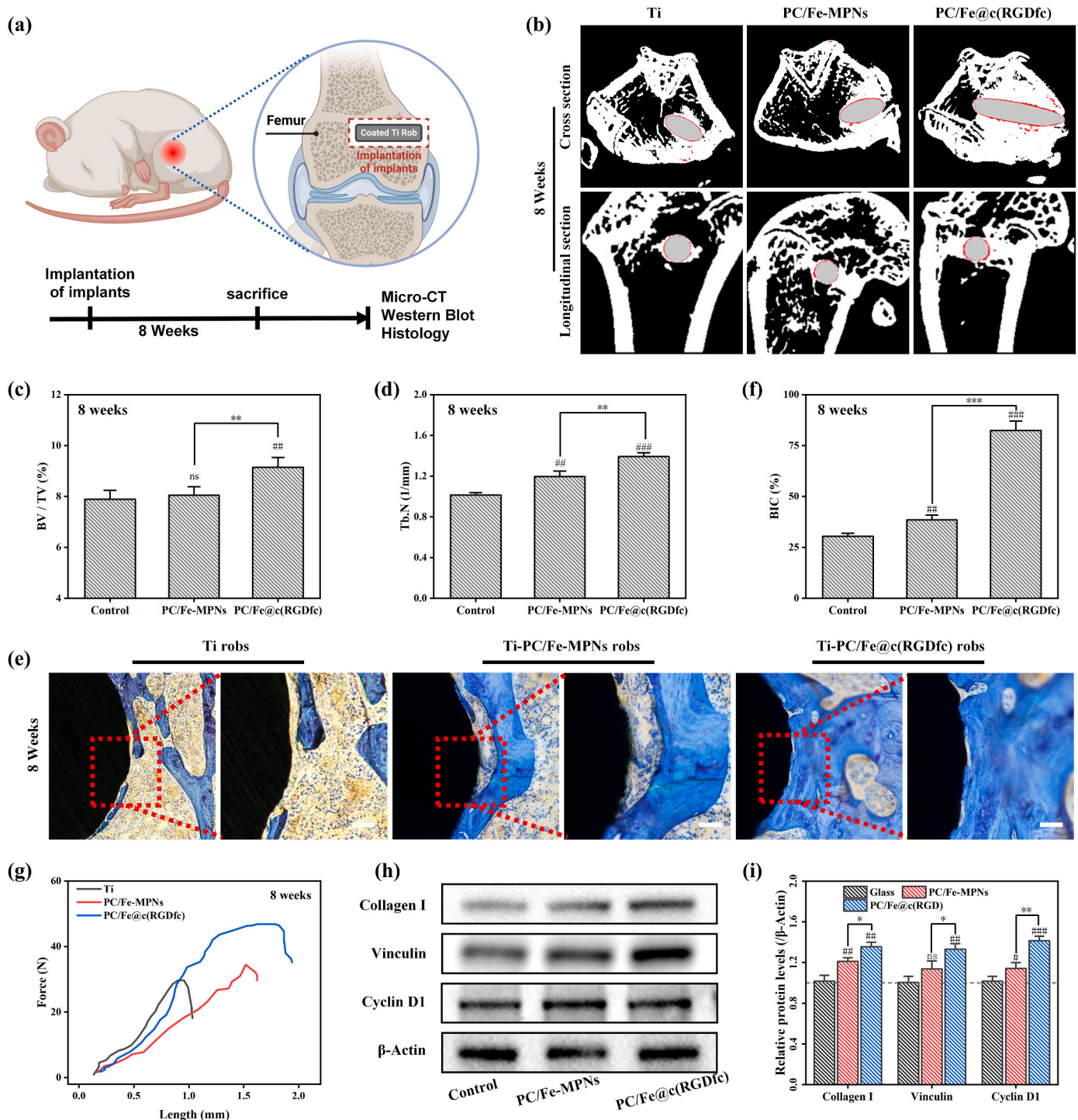


Fig. 9. Osteoinductive and osseointegration capacities of functionalized Ti-based materials in vivo. (a) Schematic diagram of the experiment in vivo. (b) Micro-CT was used to detect the quality of the regenerated bone around the implanted Ti rods containing different coatings after 8 weeks. (c) Comparison of the bone volume fraction (BV/TV %) of the implants of (b). (d) Comparison of the trabecular number (Tb.N 1/mm) of the implants of (b). (e) Representative histological images of Ti rod coated different coatings stained with toluidine blue. (f) The average histomorphometric values of bone-implant contact (BIC). Scale bars in (e) are 100 μm. N = 3, no significance noted as "ns", ***p < 0.001 using *t*-test. n = 3, no significance noted as "ns," *p < 0.05, **p < 0.01, ***p < 0.001, and #p < 0.05, ##p < 0.01 or ###p < 0.001 compared with the Control group, using *t*-test. (Schematic illustration created with [BioRender.com](https://www.biorender.com)). (For interpretation of the references to color in this figure legend, the reader is referred to the Web version of this article.)

osteogenesis (blue staining) at either 4 or 8 weeks, whereas there was the less neo-bone formation on the bare Ti and Ti-(PC/Fe)₁₀-MPNs, and the Ti rods were the worst. Although there are feeble bone mineral deposits on the surface of Ti and Ti-(PC/Fe)₁₀-MPNs, the distribution is scattered and not compact. Quantitative analysis showed that the BIC of

the Ti-(PC/Fe)₁₀@c(RGDfc) rods (82.754%) were 2.71 and 2.15 times as the bare Ti rods (30.468%) and Ti-(PC/Fe)₁₀-MPNs (38.484%) at 8 weeks, indicating that the Ti-(PC/Fe)₁₀@c(RGDfc) implant can promote better bone-implant integration. In addition, enhanced osseointegration was confirmed by biomechanical pull-out testing (Fig. 9g). Ti-(PC/

Fe)₁₀@c(RGDfc) robs were firmly connected to the surrounding bone tissue and require greater force to pull them out, while in Ti and Ti-(PC/Fe)₁₀-MPNs robs were weakly connected and required lesser to remove them.

Mechanistically, western blots (WB) showed that the bone tissue around Ti-(PC/Fe)₁₀@c(RGDfc) exhibited higher expression levels of Collagen I, cell proliferation-related protein (Cyclin D1) and cell adhesion-related protein (Vinculin) (Fig. 9h and i). Among them, Vinculin plays a crucial role in cell-cell and cell-matrix adhesion [61]. It can form a complex with the cell adhesion molecules of the actin cytoskeleton, calmodulin, and integrin family, promoting the tight attachment of cells to the substrate [62]. Thus, the excellent cell adhesion properties of PC/Fe@c(RGDfc) complex coatings may be attributed to high expression of adhesion phenotypic proteins such as Vinculin. Cyclin D1 is a cell cycle protein that plays a crucial role in the progression of the G1 phase of the cell cycle [63]. Cyclin D1 binds and activates CDK4/6 (Cyclin Dependent Kinase 4/6), thereby promoting DNA synthesis and proliferation in G1-phase cells [64]. Overall, the PC/Fe@c(RGDfc) composite coating effectively preserved the function of RGD as a part of the extracellular matrix (ECM), which can bind to integrin receptors on the cell surface and effectively upregulate the expression of genes related to cell proliferation, adhesion and osteogenic differentiation. The above results suggest that Ti-(PC/Fe)₁₀@c(RGDfc) has good tissue integration ability in vivo and promotes bone repair.

4. Conclusion

In conclusion, c(RGDfc) was successfully immobilized onto implant through the simple and efficient thiol-click reaction between cysteine in c(RGDfc) and quinones groups rich in PC/Fe-MPNs to accelerate implant osteointegration. No matter with the beneath layer, only the top layer of PC/Fe-MPNs is chemical active for immobilization of c(RGDfc), resulting in a constant coating thickness of c(RGDfc), about 12.4 ± 2.04 nm. PC/Fe@c(RGDfc) has similar roughness to PC/Fe-MPNs, but more hydrophilic, higher Young's modulus and higher adhesive energy than those of PC/Fe-MPNs. Inheriting anti-inflammatory and antioxidant of PC/Fe-MPNs, PC/Fe@c(RGDfc) can promote the proliferation, adhesion, and migration of different types of cells on the implant surface while also reducing cell damage caused by high oxidative stress. Importantly, PC/Fe@c(RGDfc) enhanced bone regeneration and integration after femoral defects in mice. Capitalizing on potent functions of peptides and the general coating ability of MPNs with a wide range of applicable metal ions and polyphenols, we believe this modification strategy provides a novel and effective strategy for further modifying MPN coatings with potential biological applications.

Formatting of funding sources

This work was supported by Start-up Funding from Wenzhou Institute, University of Chinese Academy of Science (WIUCASQD2021032). Medical Health Science and Technology Project of Zhejiang Provincial Health Commission, China (2024KY144, 2023RC207), the Wenzhou Public Welfare Science and Technology Research Project (Y20210436), National Natural Science Foundation of China (82302698).

CRedit authorship contribution statement

Zeyu Shou: Writing – review & editing, Writing – original draft, Methodology, Investigation. **Zhibiao Bai:** Writing – original draft, Methodology, Formal analysis, Conceptualization. **Kaiyuan Huo:** Software, Resources, Data curation. **Shengwu Zheng:** Resources, Methodology. **Yizhe Shen:** Writing – original draft. **Han Zhou:** Project administration, Formal analysis. **Xiaojing Huang:** Supervision, Project administration, Conceptualization. **Hongming Meng:** Writing – original draft, Validation. **Chenwei Xu:** Writing – original draft. **Shaohao Wu:** Visualization, Supervision. **Na Li:** Writing – review & editing, Writing –

original draft, Investigation, Conceptualization. **Chun Chen:** Visualization, Supervision, Resources, Project administration, Conceptualization.

Declaration of competing interest

The authors declare that they have no known competing financial interests or personal relationships that could have appeared to influence the work reported in this paper.

Data availability

Data will be made available on request.

Appendix A. Supplementary data

Supplementary data to this article can be found online at <https://doi.org/10.1016/j.mtbio.2024.101017>.

References

- [1] A. Revathi, A.D. Borrás, A.I. Muñoz, et al., Degradation mechanisms and future challenges of titanium and its alloys for dental implant applications in oral environment, *Mater. Sci. Eng., C* 76 (2017) 1354–1368.
- [2] Y. Zhu, D. Zhou, X. Zan, et al., Engineering the surfaces of orthopedic implants with osteogenesis and antioxidants to enhance bone formation in vitro and in vivo, *Colloids Surf. B Biointerfaces* 212 (2022) 112319.
- [3] M. Mehta, K. Schmidt-Bleek, G.N. Duda, et al., Biomaterial delivery of morphogens to mimic the natural healing cascade in bone, *Adv. Drug Deliv. Rev.* 64 (2012) 1257–1276.
- [4] Z. Bai, K. Hu, Z. Shou, et al., Layer-by-layer assembly of procyanidin and collagen promotes mesenchymal stem cell proliferation and osteogenic differentiation in vitro and in vivo, *Regen Biomater* 10 (2023) rbac107.
- [5] A. Shekaran, A.J. García, Extracellular matrix-mimetic adhesive biomaterials for bone repair, *J. Biomed. Mater. Res.* 96 (2011) 261–272.
- [6] X.X. Cheng, Y.X. Zhu, S.C. Tang, et al., Material priority engineered metal-polyphenol networks: mechanism and platform for multifunctionalities, *J. Nanobiotechnol.* 20 (2022) 18.
- [7] H. Ejima, J.J. Richardson, K. Liang, et al., One-step assembly of coordination complexes for versatile film and particle engineering, *Science* 341 (2013) 154–157.
- [8] H. Ejima, J.J. Richardson, K. Liang, et al., One-step assembly of coordination complexes for versatile film and particle engineering, *Science* 341 (2013) 154–157.
- [9] J. Bijlsma, W.J.C. de Bruijn, K.P. Velikov, et al., Unravelling discoloration caused by iron-flavonoid interactions: complexation, oxidation, and formation of networks, *Food Chem.* 370 (2022) 131292.
- [10] H. Geng, Q.Z. Zhong, J. Li, et al., Metal ion-directed functional metal-phenolic materials, *Chem. Rev.* 122 (2022) 11432–11473.
- [11] M. Abbas, F. Saeed, F.M. Anjum, et al., Natural polyphenols: an overview, *Int. J. Food Prop.* 20 (2017) 1689–1699.
- [12] Y.X. Guo, Q. Sun, F.G. Wu, et al., Polyphenol-containing nanoparticles: synthesis, properties, and therapeutic delivery, *Adv. Mater.* 33 (2021) 36.
- [13] S. Lee, Y.Y. Chang, J. Lee, et al., Surface engineering of titanium alloy using metal-polyphenol network coating with magnesium ions for improved osseointegration, *Biomater. Sci.* 8 (2020) 3404–3417.
- [14] Y. Wang, Y. He, Q. Wang, et al., Microporous membranes for ultrafast and energy-efficient removal of antibiotics through polyphenol-mediated nanointerfaces, *Matter* 6 (2023) 260–273.
- [15] H.M. Geng, L.P. Zhuang, M.Q. Li, et al., Interfacial assembly of metal-phenolic networks for hair dyeing, *ACS Appl. Mater. Interfaces* 12 (2020) 29826–29834.
- [16] X. Li, P. Gao, J. Tan, et al., Assembly of metal-phenolic/catecholamine networks for synergistically anti-inflammatory, antimicrobial, and anticoagulant coatings, *ACS Appl. Mater. Interfaces* 10 (2018) 40844–40853.
- [17] M. Asgari, Y. Yang, S. Yang, et al., Mg-phenolic network strategy for enhancing corrosion resistance and osteocompatibility of degradable magnesium alloys, *ACS Omega* 4 (2019) 21931–21944.
- [18] Y. Yu, X. Wang, Y. Zhu, et al., Is polydopamine beneficial for cells on the modified surface? *Regen Biomater* 9 (2022) rbac078.
- [19] X. Liao, G. Gong, M. Dai, et al., Systemic tumor suppression via macrophage-driven automated homing of metal-phenolic-gated nanosponges for metastatic melanoma, *Adv. Sci.* 10 (2023) e2207488.
- [20] Y. Zhang, L. Shen, Q.Z. Zhong, et al., Metal-phenolic network coatings for engineering bioactive interfaces, *Colloids Surf. B Biointerfaces* 205 (2021) 111851.
- [21] Y. Xu, Y. Guo, C. Zhang, et al., Fibronectin-coated metal-phenolic networks for cooperative tumor chemo-/chemodynamic/immune therapy via enhanced ferroptosis-mediated immunogenic cell death, *ACS Nano* 16 (2022) 984–996.
- [22] Y. Zhang, K. Li, L. Shen, et al., Metal phenolic nanodressing of porous polymer scaffolds for enhanced bone regeneration via interfacial gating growth factor release and stem cell differentiation, *ACS Appl. Mater. Interfaces* 14 (2022) 268–277.

- [23] Y. Oz, A. Barras, R. Sanyal, et al., Functionalization of reduced graphene oxide via thiol-maleimide "click" chemistry: facile fabrication of targeted drug delivery vehicles, *ACS Appl. Mater. Interfaces* 9 (2017) 34194–34203.
- [24] C.E. Hoyle, A.B. Lowe, C.N. Bowman, Thiol-click chemistry: a multifaceted toolbox for small molecule and polymer synthesis, *Chem. Soc. Rev.* 39 (2010) 1355–1387.
- [25] J. Sun, Y. Huang, H. Zhao, et al., Bio-clickable mussel-inspired peptides improve titanium-based material osseointegration synergistically with immunopolarization-regulation, *Bioact. Mater.* 9 (2022) 1–14.
- [26] H. Zhao, Y. Huang, W. Zhang, et al., Mussel-Inspired peptide coatings on titanium implant to improve osseointegration in osteoporotic condition, *ACS Biomater. Sci. Eng.* 4 (2018) 2505–2515.
- [27] Y. Han, R.P.M. Lafleur, J. Zhou, et al., Role of molecular interactions in supramolecular polypeptide-polyphenol networks for engineering functional materials, *J. Am. Chem. Soc.* 144 (2022) 12510–12519.
- [28] L. Wu, Y. Kim, G.M. Seon, et al., Effects of RGD-grafted phosphatidylserine-containing liposomes on the polarization of macrophages and bone tissue regeneration, *Biomaterials* 279 (2021) 121239.
- [29] S.C. Tao, X.R. Li, W.J. Wei, et al., Polymeric coating on beta-TCP scaffolds provides immobilization of small extracellular vesicles with surface-functionalization and ZEB1-Loading for bone defect repair in diabetes mellitus, *Biomaterials* 283 (2022) 121465.
- [30] M.A. Dechantsreiter, E. Planker, B. Mathä, et al., N-Methylated cyclic RGD peptides as highly active and selective alpha(V)beta(3) integrin antagonists, *J. Med. Chem.* 42 (1999) 3033–3040.
- [31] L. Duque-Sanchez, N. Brack, A. Postma, et al., Engineering the biointerface of electrospun 3D scaffolds with functionalized polymer brushes for enhanced cell binding, *Biomacromolecules* 20 (2019) 813–825.
- [32] F. Hamdan, Z. Bigdeli, S.M. Asghari, et al., Synthesis of modified RGD-based peptides and their in vitro activity, *ChemMedChem* 14 (2019) 282–288.
- [33] F. Fang, Y. Ni, H. Yu, et al., Inflammatory endothelium-targeted and cathepsin responsive nanoparticles are effective against atherosclerosis, *Theranostics* 12 (2022) 4200–4220.
- [34] N. Li, Z. Shou, S. Yang, et al., Subtle distinction in molecular structure of flavonoids leads to vastly different coating efficiency and mechanism of metal-polyphenol networks with excellent antioxidant activities, *Colloids Surf. B Biointerfaces* 229 (2023) 113454.
- [35] X. Cheng, Y. Zhu, S. Tang, et al., Material priority engineered metal-polyphenol networks: mechanism and platform for multifunctionalities, *J. Nanobiotechnol.* 20 (2022) 255.
- [36] X. Cheng, R. Lu, X. Zhang, et al., Silanization of a metal-polyphenol coating onto diverse substrates as a strategy for controllable wettability with enhanced performance to resist acid corrosion, *Langmuir* 37 (2021) 3637–3647.
- [37] J. Kroll, H.M. Rawel, S. Rohn, Reactions of plant phenolics with food proteins and enzymes under special consideration of covalent bonds, *Food Sci. Technol. Res.* 9 (2003) 205–218.
- [38] Z. Shou, Z. Bai, H. Zhou, et al., Engineering tunable dual peptide hybrid coatings promote osseointegration of implants, *Mater Today Bio* 24 (2024) 100921.
- [39] Z. Bai, K. Hu, Z. Shou, et al., Engineering a mucin coating to promote osteogenic differentiation of BMSCs in vitro and bone formation in vivo through the Wnt/ β -catenin pathway, *Colloids Surf. B Biointerfaces* 221 (2023) 113000.
- [40] M.I. Flamini, G.V. Gauna, M.L. Sottile, et al., Retinoic acid reduces migration of human breast cancer cells: role of retinoic acid receptor beta, *J. Cell Mol. Med.* 18 (2014) 1113–1123.
- [41] S. Cao, C. Wang, J. Yan, et al., Curcumin ameliorates oxidative stress-induced intestinal barrier injury and mitochondrial damage by promoting Parkin dependent mitophagy through AMPK-TFEB signal pathway, *Free Radic. Biol. Med.* 147 (2020) 8–22.
- [42] Z. Wu, M. Zhang, F. Cui, Adhesion and growth of smooth muscle cells on CNx coatings, *Surf. Coating. Technol.* 201 (2007) 5710–5715.
- [43] B. Bouchet-Fabre, G. Lazar, D. Ballutaud, et al., Influence on the sp³/sp² character of the carbon on the insertion of nitrogen in RFMS carbon nitride films, *Diam. Relat. Mater.* 17 (2008) 700–704.
- [44] F. Liu, C. Ma, Y. Gao, et al., Food-grade covalent complexes and their application as nutraceutical delivery systems: a review, *Compr. Rev. Food Sci. Food Saf.* 16 (2017) 76–95.
- [45] T.H. Quan, S. Benjakul, T. Sae-leaw, et al., Protein–polyphenol conjugates: antioxidant property, functionalities and their applications, *Trends Food Sci. Technol.* 91 (2019) 507–517.
- [46] T. Ishii, T. Mori, T. Tanaka, et al., Covalent modification of proteins by green tea polyphenol (-)epigallocatechin-3-gallate through autoxidation, *Free Radic. Biol. Med.* 45 (2008) 1384–1394.
- [47] T. Ishii, T. Mori, T. Tanaka, et al., Covalent modification of proteins by green tea polyphenol (-)epigallocatechin-3-gallate through autoxidation, *Free Radic. Biol. Med.* 10 (2008) 1384–1394.
- [48] M.P. Monopoli, D. Walczyk, A. Campbell, et al., Physical-chemical aspects of protein corona: relevance to in vitro and in vivo biological impacts of nanoparticles, *J. Am. Chem. Soc.* 133 (2011) 2525–2534.
- [49] Y. Li, S. Jongberg, M.L. Andersen, et al., Quinone-induced protein modifications: kinetic preference for reaction of 1,2-benzoquinones with thiol groups in proteins, *Free Radic. Biol. Med.* 97 (2016) 148–157.
- [50] F.H. Schunemann, M.E. Galarraga-Vinueza, R. Magini, et al., Zirconia surface modifications for implant dentistry, *Mater. Sci. Eng., C* 98 (2019) 1294–1305.
- [51] S. Seang, P. Pavasant, V. Everts, et al., Prostacyclin analog promotes human dental pulp cell migration via a matrix metalloproteinase 9–related pathway, *J. Endod.* 45 (2019) 873–881.
- [52] S.A. Kamranvar, B. Rani, S. Johansson, Cell cycle regulation by integrin-mediated adhesion, *Cells* (2022) 11.
- [53] P. Terry, K. Bilchick, C.A. Campbell, Use of acellular biologic matrix envelope for cardiac implantable electronic device placement to correct migration into submuscular breast implant pocket, *Arch Plast Surg* 50 (2023) 156–159.
- [54] L. Chen, J.M. McCrete, J.C. Lee, et al., The role of surface charge on the uptake and biocompatibility of hydroxyapatite nanoparticles with osteoblast cells, *Nanotechnology* 22 (2011) 105708.
- [55] A.A. Khalili, M.R. Ahmad, A review of cell adhesion studies for biomedical and biological applications, *Int. J. Mol. Sci.* 16 (2015) 18149–18184.
- [56] H. Lu, Y. Liu, J. Guo, et al., Biomaterials with antibacterial and osteoinductive properties to repair infected bone defects, *Int. J. Mol. Sci.* 17 (2016) 334.
- [57] Q. Fang, S. Guo, H. Zhou, et al., Astaxanthin protects against early burn-wound progression in rats by attenuating oxidative stress-induced inflammation and mitochondria-related apoptosis, *Sci. Rep.* 7 (2017) 1–13.
- [58] Z. Bai, K. Hu, Z. Shou, et al., Engineering a mucin coating to promote osteogenic differentiation of BMSCs in vitro and bone formation in vivo through the Wnt/ β -catenin pathway, *Colloids Surf. B Biointerfaces* 221 (2023) 113000.
- [59] M.J. Rahman, A. Costa de Camargo, F. Shahidi, Phenolic profiles and antioxidant activity of defatted camelina and sophia seeds, *Food Chem.* 240 (2018) 917–925.
- [60] K.M. Sharp, R. Higuchi-Sanabria, G.A. Timblin, et al., Adhesion-mediated mechanosignaling forces mitohormesis, *Cell Metabol.* 33 (2021) 1322–1341. e1313.
- [61] K.J. Shields, M.J. Beckman, G.L. Bowlin, et al., Mechanical properties and cellular proliferation of electrospun collagen type II, *Tissue Eng.* 10 (2004) 1510–1517.
- [62] J.L. Bays, K.A. DeMali, Vinculin in cell-cell and cell-matrix adhesions, *Cell. Mol. Life Sci.* 74 (2017) 2999–3009.
- [63] C.F. Welsh, K. Roovers, J. Villanueva, et al., Timing of cyclin D1 expression within G1 phase is controlled by Rho, *Nat. Cell Biol.* 3 (2001) 950–957.
- [64] C. Ma, D. Wang, Z. Tian, et al., USP13 deubiquitinates and stabilizes cyclin D1 to promote gastric cancer cell cycle progression and cell proliferation, *Oncogene* (2023).